NASA CR-169,832

NASA-CR-169832
19830009231

A Reproduced Copy

OF

NASA CR - 169, 832

Reproduced for NASA

by the

NASA Scientific and Technical Information Facility

FFNo 672 Aug 65

NASA Contractor Report

CR- 169, 832

AD

(NASA-CR-169832) INTERPRETATION OF 2-PROBE TURBULENCE MEASUREMENTS IN AN AXISYMMETRIC CONTRACTION Final Report (Illinois Inst. of Tech.) 74 p HC A04/MF A01 CSCL 01A

N83-17502

Unclas
G3/02 02681

Illinois Institute of Technology, Chicago, Illinois 60616

INTERPRETATION OF TWO-PROBE TURBULENCE MEASUREMENTS IN AN AXISYMMETRIC CONTRACTION

by

C. Marion-Moulin, J. Tan-atichat
and H. M. Nagib

IIT Fluids & Heat Transfer Report R83-1

January, 1983

Supported under NASA Grant NSG-3220

N83-17502 #

TABLE OF CONTENTS

PRECEDING PAGE BLANK NOT FILMED

LIST OF FIGURES

LIST OF SYMBOLS

Symbol	Definition
C	Contraction area ratio = (inlet area)/(outlet area)
L	Contraction length
L_{ur}	Lateral integral length scale based on the streamwise velocity component
L_{ux}	Longitudinal integral length scale based on the streamwise velocity component
L_{vr}	Lateral integral length scale based on the radial velocity component
L_{vx}	Longitudinal integral length scale based on the radial velocity component
q'	Root-mean-square of total turbulence kinetic energy
r	Distance from axis of symmetry
R(x)	Radius of contraction contour at x
U	Streamwise velocity
$\bar{U}$	Streamwise mean velocity
u'	Root-mean-square of velocity fluctuations in the streamwise direction
V	Radial velocity
$\bar{V}$	Radial mean velocity
v'	Root-mean-square of velocity fluctuations in the radial direction
$\overline{uv}$	Reynolds stress between streamwise component of velocity and a component normal to the axis of symmetry

Symbol	Definition
μ_u	Streamwise turbulence kinetic energy ratio $= u_e'^2/u_i'^2$
μ_v	Radial turbulence kinetic energy ratio $= v_e'^2/v_i'^2$
σ	Grid solidity = (closed area)/(total area)
τ	Time delay in auto- and cross-correlation functions

Subscript	Definition
e	Value at exit of contraction
i	Value at inlet of contraction
$(\bar{\ })$	Overbar = average value, time-average value

ABSTRACT

Simultaneous measurements of the streamwise and radial velocity components at two points, one on and one off the centerline with variable radial separation, were digitally recorded and processed at several stations along a four to one contraction with controlled upstream turbulence conditions. Various statistical quantities are presented including spectra and coherence functions. The integral scales L_{ux}, L_{ur}, L_{vx} and L_{vr} were also estimated and their variation along the contraction is examined. While the results agree with the predictions of rapid distortion theory on the axis, the discrepancy is significant off the centerline. The experiment indicates that the off-axis kinetic energies are more sensitive to nonlinear effects than their on-axis counterparts. In addition, the theory grossly underestimates and overestimates the longitudinal integral length scales based on the streamwise velocity and the radial velocity, repsectively. The aspect ratio of the energy containing-eddies does not elongate as much as one would expect based on the rapid distortion theory or on simple geometrical considerations. In fact, when nondimensionalized by the local radius of the contraction, the length scales still increase. That is, the energy-containing eddy takes more room relative to the available space, even though the flow itself

contracts. This refutes the previously proposed mechanism based on distortion of "atmospheric turbulence" for the generation of persistent and slender disturbances that lead to blade-passing noise generation in ground testing of jet engines.

CHAPTER I

INTRODUCTION

The study of the behavior of turbulence in an axisymmetric contraction is of great practical interest. It is known that the distortion of a free stream alters the characteristics, length scales as well as intensities, of the turbulence that is convected by the mean flow through a contraction. The elongation in the streamwise direction of the turbulent eddies when the flow is sucked into a stationary jet engine has been considered as responsible for pure-tone noise generation. Contractions are also used by wind-tunnel designers because it is an efficient means of reducing the relative turbulence intensity in test sections. A better understanding of the mechanisms involved in the distortion of turbulence is important for use of contractions at their best possible efficiency in turbulence manipulation, and it would greatly help in the noise reduction for jet engines.

In order to document the behavior of turbulence under strain, many investigators have studied contractions by either theoretical or experimental methods. Ribner and Tucker (1953) and Batchelor and Proudman (1954) derived the so-called classical rapid distortion theory which predicts the variations of turbulent intensities as a function of the contraction ratio, starting from isotropic turbulence. Recently, Chen (1981) also studied the radial development of these quantities, along with integral length scales, by including vortex bending and tilting, using the methods developed by Hunt (1973), and by Goldstein (1978, 1979). It is important to recognize that all these theories are linear. Tan-atichat (1980) investigated experimentally the sensitivity of the performance of various contractions to different initial integral length scales, which previously was not documented. For a review of earlier experimental investigations, see Tan-atichat (1980). He also studied the decay of turbulence in a straight duct, and showed that when corrected for viscous decay a close agreement exists between experimental values and the predictions of classical rapid distortion theory for mild contractions.

Although Tan-atichat (1980) measured off-axis data, only the data taken on the centerline of the contraction were analyzed in detail in that study. The present study is a further analysis of the data obtained by Tan-atichat (1980). In particular, we focus in this study on two-probe, two-component, simultaneous data that he obtained in a four to one contraction for one of his test flow conditions, but did not analyze. The question of interest here deals with the deformation of the energy containing eddies by the contraction. In order to analyze this, the lateral integral length scales have to be calculated from his simultaneous measurements using two probes with varying radial separation. Also, the radial dependency of the turbulence intensities, longitudinal integral length scales, and velocity spectra are extracted from these two-probe measurements. The results are compared with the predictions of rapid distortion theory (Chen, 1981).

The main objective of the present work is to establish the degree to which linear estimates of contracting flows are valid. Tan-atichat (1980) revived the interest in such theories when he discovered that simple corrections for viscous decay, which had been ignored in all previous experimental studies, can bring about remarkably close agreement between experiments and theory for measurements on the axis of symmetry. However, conditions away from this centerline are far more important.

The secondary objective here is to determine the role of the contraction in distorting turbulence eddies; a question of great significance to the fan intake problem. Such understanding is essential for the design of inflow control devices and of wind-tunnel turbulence manipulators.

The authors would like to thank Lennart S. Hultgren for all the stimulating discussions and for his valuable comments on the drafts of this report. This study has been supported by the NASA Lewis Research Center under

Grant NSG-3220, monitored by John Groeneweg. Partial support was also provided by NASA Langley Research Center under Grant NAG-1-74.

CHAPTER II

TAN-ATICHAT AND NAGIB'S EXPERIMENTAL DATA

Tan-atichat's (1980) investigation was conducted in an open-circuit wind tunnel, powered by a compressed air supply. The compressed air was fed into a settling chamber via an acoustically treated duct. The settling chamber contained an array of turbulence manipulators of different types and mesh sizes, designed according to Loehrke and Nagib (1972), to reduce the absolute turbulence level and to obtain a uniform mean flow. A 25 to 1 contraction connected the settling chamber to the test section. The test section consisted of a turbulence-generating grid, a straight duct section, and a contraction followed by a smaller straight duct section. Tan-atichat (1980) considered many combinations of turbulence-generating grids and contractions. Only one of these is used here, i.e., grid J4 and the contraction C2 which has a 4 to 1 area ratio. The turbulence-generating grid (labeled J4 by Tan-atichat, 1980) was manufactured by the punched plate method and had round holes arranged in a triangular array. The mesh size was 1.745 cm. The grid had a low solidity, $\sigma =$ 0.36, such that there would be no danger of anomalous behavior (Tan-atichat et al., 1982). The straight duct, leading up to the contraction, had an internal diameter of 15.4 cm. Its length, 43.2 cm, was chosen such that the generated turbulence became homogeneous and approximately isotropic at its exit. The contraction which followed had an area ratio of four to one and a length-to-inlet diameter ratio equal to unity. The shape of the contraction was given by two third-order polynomials matched at the inflection point of the contraction. The coefficients were determined such that the radius and the slope are continuous at the inlet, the inflection point, and the exit.

The hot-wire probes were mounted on a three-dimensional traversing mechanism, capable of positioning the probes to within 0.2 mm of the required coordinates. The signals were fed into two pairs of DISA anemometers working at an overheat ratio of 1.7. Analog preprocessing of the output of the anemometers was necessary in order to achieve maximum signal-to-noise ratios, and to prevent aliasing in the calculation of spectra and correlations. Since the analog-to-digital converter of the acquisition computer covers a range of 10 volts with 12 bits, the smallest increment in voltage it can discern is about 5 mV. The output from the hot-wire probes in a typical flow situation consists of a mean DC component of several volts and a small superimposed AC component of only a few millivolts. If turbulence statistics were computed from digitization of preprocessed hot-wire signals, a poor signal-to-noise ratio would be obtained. To minimize the quantization errors, the DC component was subtracted from the hot-wire signal, and the resulting signal was amplified to utilize the full range of the converter. The bias and gain applied to the signals were recorded for each set of acquired data to allow accurate reconstruction of the original signals prior to digital linearization and processing. When four channels of signals were acquired simultaneously, the maximum sampling rate available was 11.36 kHz per channel. Therefore, the analog fourth-order Butterworth low-pass filters required to prevent aliasing were set at a cut-off frequency of 5 kHz.

Digital samples were acquired simultaneously, at four different streamwise locations, using two x-wire probes placed at six different radial positions. One probe was always located on the centerline of the four-to-one contraction. Figure 1 shows the shape of the contraction, and the location of the four streamwise planes in which data were acquired. The separation distance of the two probes ranged from 0.64 cm to 1.91 cm in 0.25 cm increments. All data were gathered with a mean velocity of 1.8 m/s as measured in the straight duct way upstream of the inlet of the contraction, i.e., Tan-atichat's (1980) test-flow condition T7a. For each combination of streamwise and radial position, a data file which consisted of 100 digital data records, each with four channels and 2048 samples was acquired.

CHAPTER III

NUMERICAL PROCESSING OF EXPERIMENTAL DATA

Each of the data files, acquired and recorded on 9-track industry standard magnetic tapes by the PDP 11/10 minicomputer, was processed on a UNIVAC - 1100/81 main-frame computer because several highly efficient signal processing software packages had been custom developed for it.

Since the anemometer voltages were DC-biased and amplified before recording them digitally to minimize quantization error for the A/D conversions, their "true" values were restored by applying the reciprocal of the gain and adding back the DC-offset values digitally in the computer. The four hot-wire signals which originated from two X-probes were converted to the streamwise, U, and radial, V, velocity components by assuming a cosine law behavior for the angular response of the X-wires using the actual geometries determined during calibration. Use of the cosine relation is justified for this experiment because the mean flow angles with respect to the probe axis were small and the turbulence intensities were low. Extraction of the required quantities was then made through the customary sum-and-difference scheme.

The first two channels represented velocity information obtained from the X-probe located along the centerline while the remaining two channels represented the velocity obtained from the off-centerline X-probe. As pointed out by Drubka and Wlezien (1979), polynomials are excellent choices for use in hot-wire calibration over a wide range of velocities, therefore squared third-order polynomials were chosen to relate the voltages to the velocities. The polynomial coefficients were computed by a least-squares routine that fits the chosen polynomial to the calibration data.

While the data from each file resided in the computer's memory after calibration, a highly efficient, general purpose fast Fourier transform (FFT) routine written in a combination of FORTRAN and UNIVAC Assembly languages was used to compute the power- and cross-spectra, coherence, phase, auto- and cross- correlations from the velocity data. These results were written onto an output tape for use by a versatile plotting program and for further processing when necessary. Concurrently, time-averaged results, such as means, variances, integral time scales and Reynolds stresses were computed from these statistical functions and printed out. These results are plotted in the figures shown in Appendix C and are discussed in the following two chapters.

CHAPTER IV

ONE-PROBE CENTERLINE RESULTS

In Tan-atichat's (1980) experiments, data were gathered also on the axis of symmetry at nine different axial locations in the same contraction using only one hot-wire probe. These measurements were not discussed in detail by Tan-atichat (1980) for the test-flow condition T7a, however. They are presented here for easy comparison with Tan-atichat's report (1981) and as a bench-mark for the two-probe data of the following chapter.

Figure 2 shows the mean streamwise velocity as a function of the axial location. In this figure, as well as in the following ones, the origin is taken to be located at the inlet of the contraction. The length, L, of the contraction is also indicated on the figures. The mean velocity increases monotonically through the contraction. As can be seen in the figure, the stream starts to contract before the solid wall does, and there is some overshoot at the outlet. The actual contraction ratio, defined as the ratio of outlet to inlet velocities, equals 3.4. The curve indicated by the crosses corresponds to the straight duct case; i.e., noncontracting flow condition.

The streamwise and radial turbulence kinetic energies are shown in Figures 3 and 4, respectively. The

ORIGINAL PAGE IS
OF POOR QUALITY

kinetic energies are normalized by their respective values at the inlet of the contraction. The constant area duct case is also shown in these figures in order to illustrate the viscous decay of turbulence in this test-flow condition. The longitudinal kinetic energy decreases monotonically with increasing values of the axial coordinate, as is expected for mild contractions. Its relative magnitude at the exit is 0.3. The lateral turbulence kinetic energy initially decreases slightly due to viscous decay, but is then amplified by the contraction. It reaches a peak value equal to 1.6 at the end of the physical contraction. By correcting these experimental results for viscous decay, a good agreement with classical rapid distortion theory (Ribner and Tucker, 1953, and Batchelor and Proudman, 1954) can be demonstrated. The correction is accomplished simply by dividing the results for the contracting case by the corresponding one for the straight-duct case (Tan-atichat, 1980). Using the actual contraction ratio, the theory predicts the following values for the turbulent kinetic energies at the exit of the contraction:

$$\mu_u = u_e'^2/u_i'^2 = 0.263$$

$$\mu_v = u_e'^2/v_i'^2 = 2.55$$

where the prime denotes the root-mean-square value of a quantity. The subscripts i and e denote the values at the inlet and the exit, respectively. The corresponding experimental values are:

$$\mu_u = (u_e'^2/u_i'^2)_{C=4} / (u_e'^2/u_i'^2)_{C=1} = 0.44$$

$$\mu_v = (u_e'^2/v_i'^2)_{C=4} / (u_e'^2/u_i'^2)_{C=1} = 2.35$$

The theory underestimates and overestimates the longitudinal and lateral kinetic energies, respectively. The total kinetic energy of turbulence is predicted fairly well by the theory, however. The evolution of the total turbulent kinetic energy along the centerline of the contraction is shown in Figure 5. The increase in the transverse components due to the contraction results in a net turbulence energy production.

The axial development of the anisotropy, defined as the ratio of the root-mean-square values of the streamwise and radial velocity components, respectively, is depicted in Figure 6. As can be seen in the figure, the incident turbulence is not perfectly isotropic. Before the contraction, as well as for all axial locations in the straight duct, the anisotropy is roughly equal to 1.2. In the contraction, the anisotropy decreases monotonically with axial distance to reach a value of 0.45 at the exit. Flagged points in Figure 6, as well as all figures included here, represent data for which no corrections related to the limited data-record size were required to estimate the integral time scales; for more details see Appendix A.

The normalized Reynolds stresses are shown in Figure 7. They are small, which is in agreement with the value of zero as predicted by the rapid distortion theory. The aberrant negative value at the very inlet of the contraction may be caused by the sudden change in curvature, but this is a remote possibility; more likely, the averaging time used in the experiment was too short to obtain stable values of this higher order statistical quantity.

Figures 8 and 9 show the streamwise integral length scale based on the axial and the radial velocity components, respectively. At the inlet of the contraction, the ratio of these integral length scales is about 1.91, which is close to the value 2.0 required for isotropic turbulence (Hinze, 1959, p. 209). The integral length scale based on the streamwise velocity, L_{ux}, decreases slightly during the first half of the contraction, but increases rapidly during the latter half. The integral length scale based on the radial velocity, L_{uv}, increases all along the contraction. The increase in this length scale is about twice as large as for the other length scale. Immediately after the physical end of the contraction, there is a sharp decrease in both integral length scales. The reason for this may lie in the method used to calculate the integral length scales. The quantities that are directly extracted from the experimental data are the integral time scales. Taylor's frozen flow hypothesis (Batchelor, 1956, p. 47) is then utilized to estimate the integral length scales. The validity of this latter procedure can be questioned inside the contraction or just downstream of it where the mean flow is not uniform.

CHAPTER V

TWO-PROBE AND OFF-CENTERLINE RESULTS

With the set of two-probe measurements described in Chapter II, it is possible to illuminate the radial evolution at four streamwise locations, of the different quantities discussed in the preceding chapter. The points at which data were acquired always utilize the same set of radial locations, c.f. Figure 1. To emphasize that the flow is contracting, it was chosen to nondimensionalize the radial distance by the local radius of the contraction.

The two probes used in the measurements had different calibrations, and, as a consequence, the data must be corrected for this probe influence. From previous results (Tan-atichat, 1980), it is known that the turbulence is nearly homogeneous and that the mean flow is uniform to a high degree at the upstream location. Thus, an attempt to reduce the error, caused by using two distinct probes was made by nondimensionalizing the measurements with the corresponding inlet values. In particular, the centerline data were scaled with the inlet centerline value, and the off-axis data were normalized by the average of the upstream off-axis values.

The mean streamwise velocity, $\bar{U}$, is considered in

Figure 10. The difficulties encountered in dealing with two different probes can be seen: the centerline probe gives slightly higher values than the off-axis probe, but it is known that this is not a real effect in the flow. The scatter at the inlet is due to the low velocity (roughly 2 m/s) at that location. The calibration of the probes is less accurate in that range. One finds, again, that the actual contraction ratio is about 3.4.

From Figure 11, which represents the angle of inclination of the streamlines with respect to the axis of symmetry, one can conclude that in the central part of the contraction the transverse mean velocity, $\bar{V}$, is very small compared with the mean streamwise velocity, $\bar{U}$. The angles are very small, except close to and along the wall where the flow has to follow the solid boundary. It can be seen that for the two middle locations, the flow is converging at the same rate along all radial positions. The non-zero values for $\tan^{-1}(\bar{V}/\bar{U})$ at the inlet and at the exit indicate that the flow has already started to contract at the entrance and is still contracting slightly at the outlet. From a similar graph, it was initially found that the second probe gave angles consistently four degrees too high compared to the other probe, which was known to be well aligned along the axis of symmetry. A correction on all measured quantities corresponding to the four degrees was then applied everywhere for the second probe.

Two of the three components of the turbulence kinetic energy are shown in Figures 12 and 13. The problem of using two different probes is evident once more. All the values on the centerline seem consistently higher than what they most likely should be, as inferred from the results by the other probe. But here, the radial evolution relies only on the off-axis probe, and the off-axis results are consistent. It is known (Tan-atichat, 1980) that the centerline values agree very well with the rapid distortion theory for this contraction when a correction for the viscous dissipation is applied. The off-axis results can also be compared with the rapid distortion theory (Chen, 1981) at the exit. Here, the viscous correction is applied to the theory and indicated by subscript VC to the rapid distortion theory (RDT). For the longitudinal component, the theory predicts a slight decrease with radial position, instead of the slight increase found experimentally. For the lateral component, a slight increase with the radial coordinate is predicted, but the experiment shows a far more enhanced increase. The discrepancy is already visible at a radial position of about 20% of the local radius in both cases. This is probably due to nonlinear effects that are ignored in the rapid distortion theory.

The Reynolds stresses are shown in Figure 14. They are all very small. There is also a lot of scatter in the experimental data, especially for the inlet locations. For the outlet locations where the velocity is higher and the hot wires are more accurate, the values are more consistent and smaller. The length of the records taken might have been too short for the averages to stabilize to consistent values, however.

The radial evolution of the longitudinal integral length scales, L_{ux} and L_{vx}, based on the streamwise and radial velocities, respectively, is shown in Figures 15 and 16. There is a lot of scatter in the estimated longitudinal integral length scales, L_{ux}, near the exit of the contraction: these scales are difficult quantities to obtain because a very small error in measuring the velocities is amplified in calculating the integral scales. At the first two stations, the flow is homogeneous and both integral scales are independent of the radial coordinate. Farther into the contraction, there is a tendency for the scales to increase with the radial distance except at one station where there is a decrease in L_{ux}. These trends are not as pronounced in the predictions by rapid distortion theory (Chen, 1981). Once more, the nonlinear effects are suspected to be responsible for the discrepancies. Moreover, the absolute level of the theoretical and experimental values are far apart from each other. It has been seen in the preceding chapter that the integral scales drop suddenly right after the contraction. That can be due either to a real relaxation of the flow, or to an improvement in the validity of Taylor's hypothesis. Taking this overestimation into account, a rectification would bring L_{ux} lower, closer to the value predicted by the rapid distortion theory, but probably not as low. On the contrary, in the L_{vx} case, the discrepancy would be accentuated.

The radial integral length scales, based on the streamwise velocity, L_{ur}, and the transverse velocity, L_{vr}, have also been calculated (c.f. Appendix B). From previous studies (Hanson, 1977) it was suggested that the aspect ratio of an energy-containing eddy would be enormously increased by a contraction. That is, the radial integral scales would shrink and the longitudinal ones would increase. It has been shown here that the latter scales increase indeed. But the former either increase or stay the same through the contraction, as can be seen from Figure 17, where the integral length scales have been nondimensionalized by their respective values at the inlet. The scale L_{ur} increases slightly, and L_{vr} remains about the same. This evolution can be checked with the rapid distortion theory (Chen, 1981), according to which L_{ur} slightly decreases and L_{vr} slightly increases. When nondimensionalized by the local radius of the contraction, as in Figure 18, the length scales still increase. That is, the energy-containing eddy takes more room relative to the available space, e[illegible] though the flow itself contracts.

Finally, the aspect ratio, based either on the streamwise velocity or the radial velocity, is shown in Figure 19. At the inlet of the contraction, these aspect ratios are very close to those for isotropic turbulence. The theory predicts that the aspect ratio based on v should remain the same, while experimentally it was found to increase. The aspect ratio based on u should increase by a factor of eight according to the theoretical predictions, but it increases by a factor of about five only. The aspect ratio based on the transverse component is the most important one for the understanding of noise generation in ducted fans.

Four different velocity spectra are shown in Figures 20 and 21, for the streamwise and the radial velocities, respectively. In each figure, spectra on the centerline at the inlet, the third axial position, and the exit are presented. In addition, the spectrum at the exit and at the farthest radial position is also shown. All of the off-axis spectra obtained here always fall, within the accuracy of the experiment, exactly on the centerline spectrum at the exit. As can be seen in Figure 20, all the transfer of energy happens between the inlet and the third measuring station. There is a net shift of energy density towards higher frequencies for the streamwise component. A corresponding trend in the spectra for the transverse component cannot be clearly identified, however.

These spectra can be compared with those predicted by the rapid distortion theory (Chen, 1981, pp. 75 and 79, respectively). One would have to use Taylor's hypothesis to transform frequencies to wave numbers, for an accurate comparison, however. Roughly speaking, one has to shift the spectra to the left in Figures 20 and 21, by the logarithm of the mean streamwise velocity, U, which is about $\log_{10} 3$. Then, it can be seen that the values obtained here are lower in the high frequency range, where the viscous dissipation occurs, which is the logical expected trend. The values in the low-frequency range are reasonably comparable. But the peak in the theoretical spectra does not appear in the experiment, this difference cannot be readily explained, and is probably due to either nonlinear effects, viscous effects, or both.

Figure 22 shows the cross-spectra between the streamwise velocities on the centerline and the first radial position, for three different downstream locations: inlet, third position x_2, and outlet. Similarly, Figure 23 shows the cross-spectra for the radial velocity between the centerline and the first radial position, for the same axial locations. It can be seen that the trends of the curves are similar to those of the u-power spectra shown in Figure 20, and the v-power spectra shown in Figure 21, thus showing the homogeneity of the flow over the given radial separation, which corresponds approximately to an integral scale.

Figures 24 through 29 show the coherences between off-axis and on-axis velocities for different radial separations, measured at three streamwise locations. Except for the largest probe separation, Figures 28 and 29, the coherence of the radial velocities is considerably larger than that for the streamwise velocity. This signifies the importance of the radial velocity, which is amplified through vortex stretching, and the nonlinear effects acting in this production process. For example, midway through the contraction, coherence levels of as large as 7% are present in the range of high frequencies over a separation distance several times the size of the radial integral scales. As expected, the decay of the coherence in the energy-containing range is exponential with frequency and is not emphasized by the linear scale used here. These results suggest the importance of the fine scales, i.e., viscous and nonlinear effects, and give us an additional clue to the differences between the rapid distortion theory and experiments even for this mild contraction, when the comparison is not limited to the centerline, as Tan-atichat's (1980) was.

CHAPTER VI

CONCLUSIONS

Simultaneous measurements of the streamwise and radial velocity components at two points, one on and one off the centerline with variable radial separation were digitally recorded and processed at several stations along a four to one contraction with controlled upstream turbulence conditions. Various statistical quantities were presented including correlation and cross correlation functions, spectra, as well as coherence functions. The integral scales L_{ux}, L_{ur}, L_{vx} and L_{vr} were also estimated and their variations along the contraction was examined.

Both the streamwise and transverse turbulence kinetic energies increase with the radial distance. This is in contrast with the quasi-homogeneous linear rapid distortion theory presented by Chen (1981). The theory predicts a milder radial increase for the transverse kinetic energy and, in fact, a decrease of the streamwise component. There are some subtle differences between the theory and the experimental setup, however. The theoretical predictions are, strictly speaking, only valid sufficiently far downstream of the contraction where the flow has become uniform again. The experimental data, used in the comparison, were acquired at the exit of the physical contraction where the mean flow is not quite uniform and the actual local contraction ratio is less than the geometrical one. Be that as it may, it is believed that the main reason for the discrepancies are nonlinear effects, however. Tan-atichat (1980) showed that centerline results, when properly corrected for viscous dissipation, agree well with the predictions of the classical rapid distortion theory for contraction ratios less than about four. This experiment indicates that the off-axis kinetic energies are more sensitive to nonlinear effects.

It is in general believed that the integral length scales of free-stream turbulence play an important role in the transition process for boundary layers. Experiments in boundary layer transition are most commonly performed downstream of a large area contraction. Also, a detailed knowledge of the behavior of those scales is needed for the optimal manipulation of turbulence in wind-tunnel design (Marion, 1983). The centerline experimental data and the theoretical results for the integral length scales show the same trends. However, a detailed comparison will suffer from the fact that it is not clear how to correct either the experimental or the theoretical results for the viscous dissipation. Keeping this in mind, a direct comparison shows that the theory grossly underestimates and overestimates the longitudinal integral length scales based on the streamwise velocity and the radial velocity, respectively. In addition, an added experimental error may have been caused by the usage of Taylor's frozen turbulence hypothesis in the estimation of one integral length scale. Both centerline lateral integral length scales are underestimated by the theory. The shape of the characteristic energy-containing eddies can be described by the aspect ratio defined as the ratio of the integral length scales. The most interesting of these is the one based on the transverse velocity component due to the amplification of that component by the contraction and the importance of that component for the jet-fan noise production problem. The experiment clearly demonstrates that both integral length scales based on the transverse velocity component increase due to the distortion. For this four to one contraction ratio, this aspect ratio is increased by a factor of five, only as compared to the theoretical prediction of eight. Therefore, only a mild elongation of the energy-containing eddies is experienced. This is in contradiction with Hanson (1977), who believed that the radial scales of atmospheric turbulence would be substantially decreased by the contraction. The aspect ratio based on the radial velocity still increases from 0.5 to about 2.5. The fact that the characteristic eddies do not shrink in the radial direction is believed to be associated with the amplification of the transverse kinetic energy by the contraction.

The shapes of the experimental one-dimensional power spectra compare well with the ones predicted by theory (Chen, 1981), except that the peak in the theoretical power spectrum for the steramwise component cannot be identified in the experiment. This may be caused by viscous effects, or nonlinear effects, or both. A comparison of the cross-spectra and the power spectra shows that the turbulence is really homogeneous in the core region.

Because of the commercially very important problem of jet-fan noise, these experimental results clearly indicate a great need for further experimental and theoretical studies of the off-axis behavior of turbulence in contracting streams. Valuable improvements in the theory would be to include effects of viscosity, nonlinear terms, or both. In future experiments on off-axis behavior it would be of interest to document a larger radial extent of the flow region, as well as the effect of larger contraction ratios.

APPENDIX A

ESTIMATION OF STREAMWISE INTEGRAL LENGTH SCALES

ESTIMATION OF STREAMWISE INTEGRAL LENGTH SCALES

The streamwise integral length scales are determined from the computed integral time scales. The integral time scales were obtained by integration of the auto-correlation function. The auto-correlation of u leads to the longitudinal streamwise integral length scale, L_{ux}, and the auto-correlation of v leads to the lateral streamwise integral length scales, L_{vx}. Corrections have been applied, when possible, to take into account the fact that the auto-correlation functions should asymptotically tend towards zero as time increases. This is because the averages of u and v are zero by definition. It may happen, due to experimental errors, that the asymptote is a small positive or negative value. Then, if the correction is not applied, the integral scales are overestimated or underestimated, respectively. These problems most probably arise due to the limited length of the acquisition records. In some cases, the asymptote was small enough and uncorrected values were used; they are shown flagged in the figures. The computer program for applying this correction was developed, optimized and documented by Wigeland (1978).

From the integral time scales, and the local mean axial velocity, $\bar{U}$, one can calculate the integral length scales by using Taylor's hypothesis, i.e.

$$L_{\alpha\beta} = \bar{U}T_{\alpha\beta}$$

where $L_{\alpha\beta}$ and $T_{\alpha\beta}$ are the integral length and time scales, respectively, in the β direction based on the α component of velocity; and $\bar{U}$ is the local mean velocity.

APPENDIX B

ESTIMATION OF RADIAL INTEGRAL LENGTH SCALES

ORIGINAL PAGE IS
OF POOR QUALITY

ESTIMATION OF RADIAL INTEGRAL LENGTH SCALES

In addition to various other statistical functions, cross-correlations between velocities off the axis of symmetry and velocities on that axis were computed from the measurements. In particular, the auto-correlations

$$R_{uu}(r) = \overline{u(o,t)u(r,t)}$$

$$R_{vv}(r) = \overline{v(o,t)v(r,t)}$$

were computed at the four axial positions. The overbar denotes ensemble average and r is the radial position. These auto-correlations can be used to calculate the lateral integral length scales on the centerline directly through

$$L_{ur} = \int_{o}^{\infty} R_{uu}(r)dr/\overline{u(o)^2}$$

$$L_{vr} = \int_{o}^{\infty} R_{vv}(r)dr/\overline{v(o)^2}$$

Because the auto-correlation can be expected to have an approximately exponential decay with radial separation, these integrals were evaluated by using a graphic method. The auto-correlations, normalized by the appropriate kinetic energy, were plotted on semi-logarithmic graph paper. Straight lines were then fitted to each set of seven data points by ocular inspection, c.f. Figure 30. The integral length scale can then be estimated from the inverse of the slope of these straight lines. For each set of data, two limiting slopes were used to obtain an error estimate of this procedure. Also, a direct planimeter integration yielded results that fall in between the ones obtained by using the limiting slopes.

APPENDIX C

FIGURES

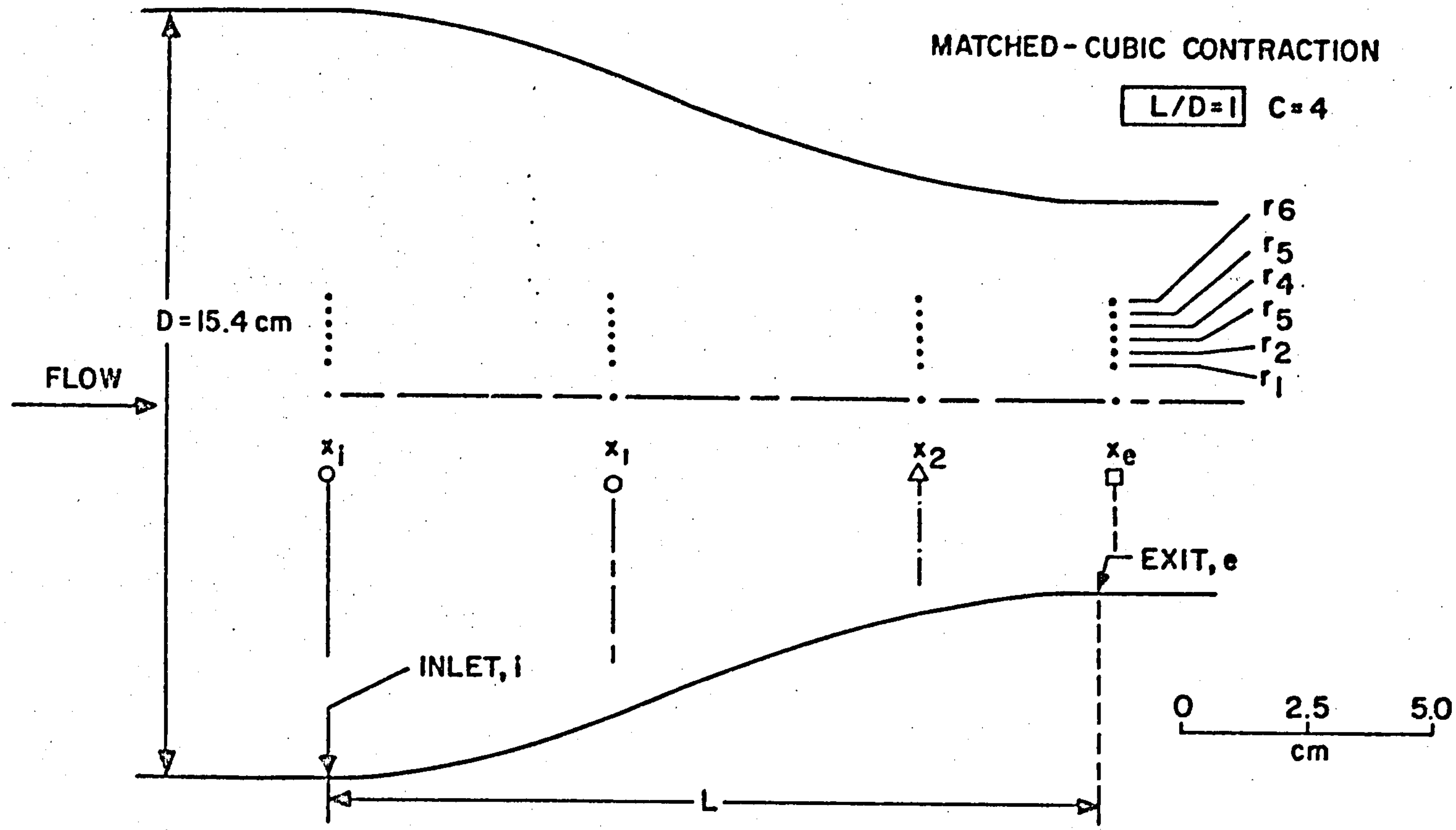

Figure 1. Positions of Data Acquisition in Contraction

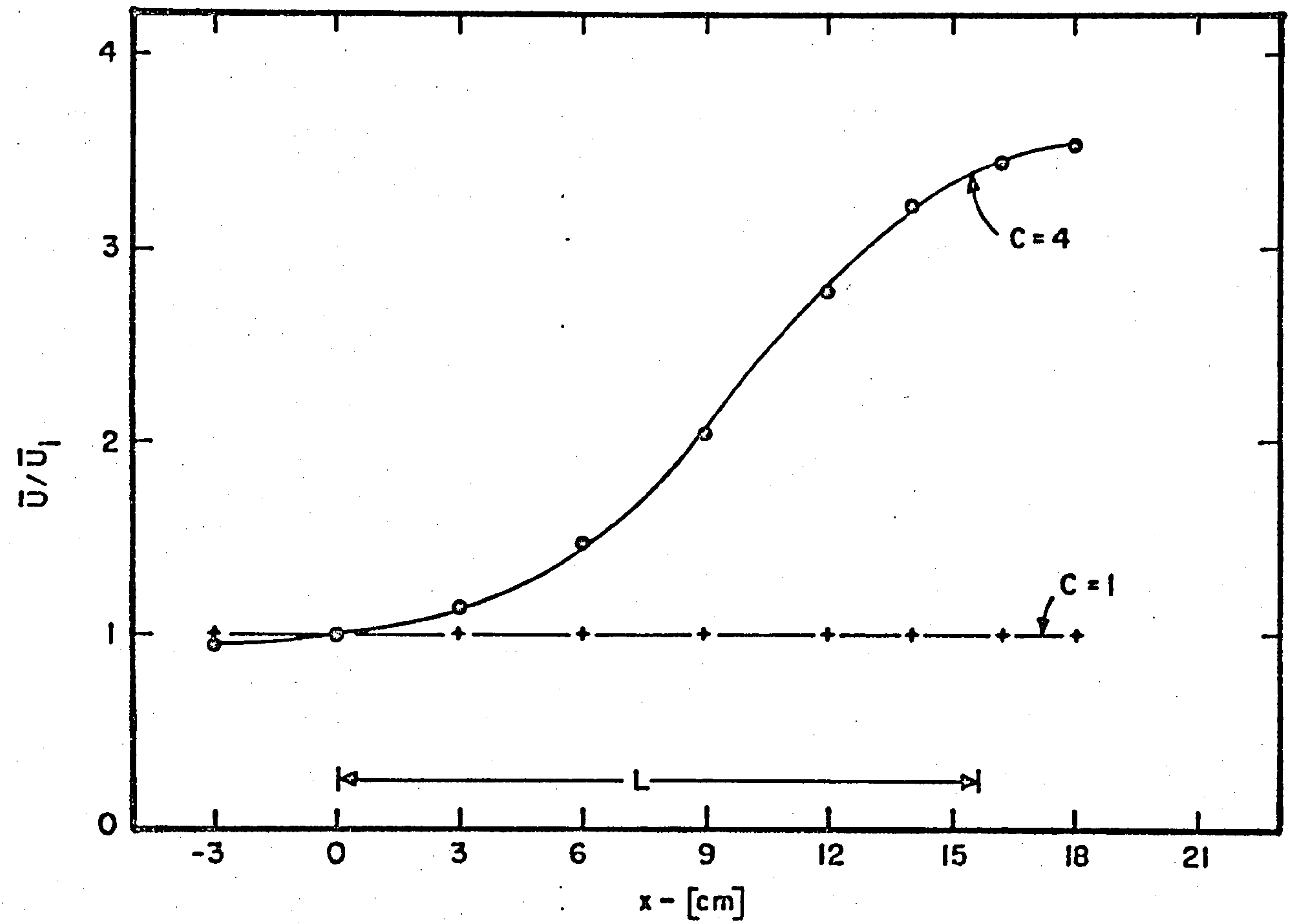

Figure 2. Streamwise Mean Velocity Along Centerline

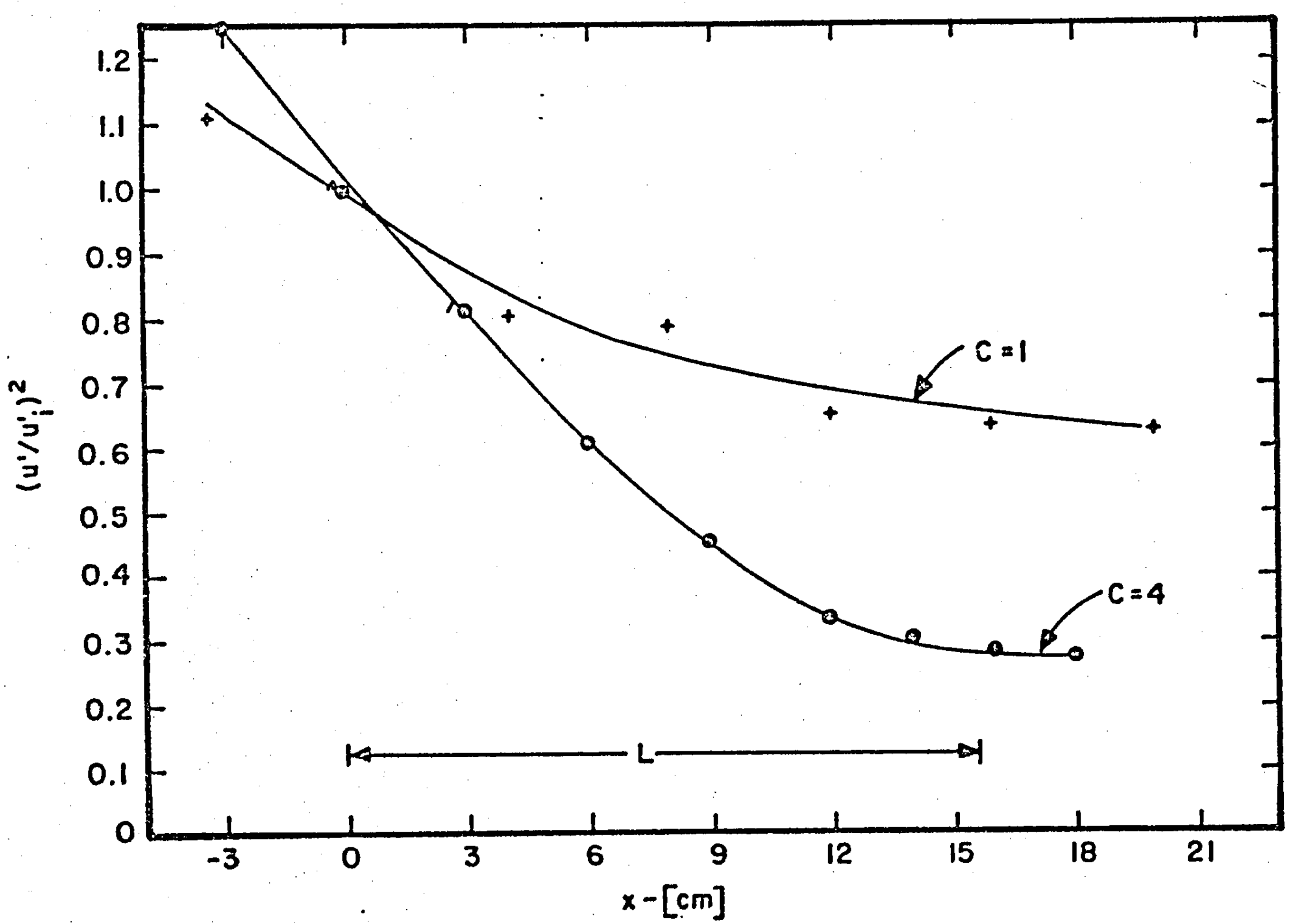

Figure 3. Streamwise Kinetic Energy Along Centerline

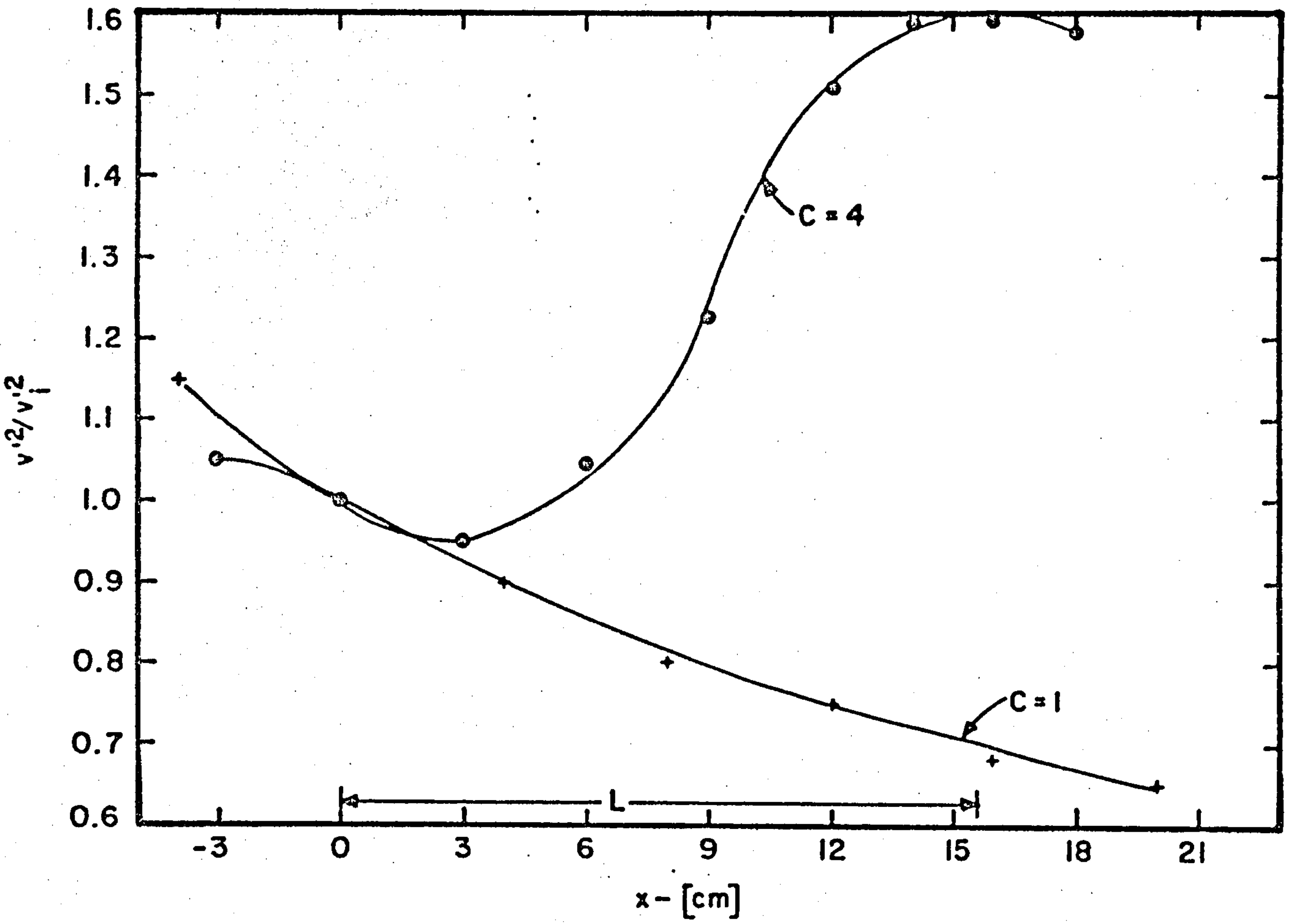

Figure 4. Transverse Kinetic Energy Along Centerline

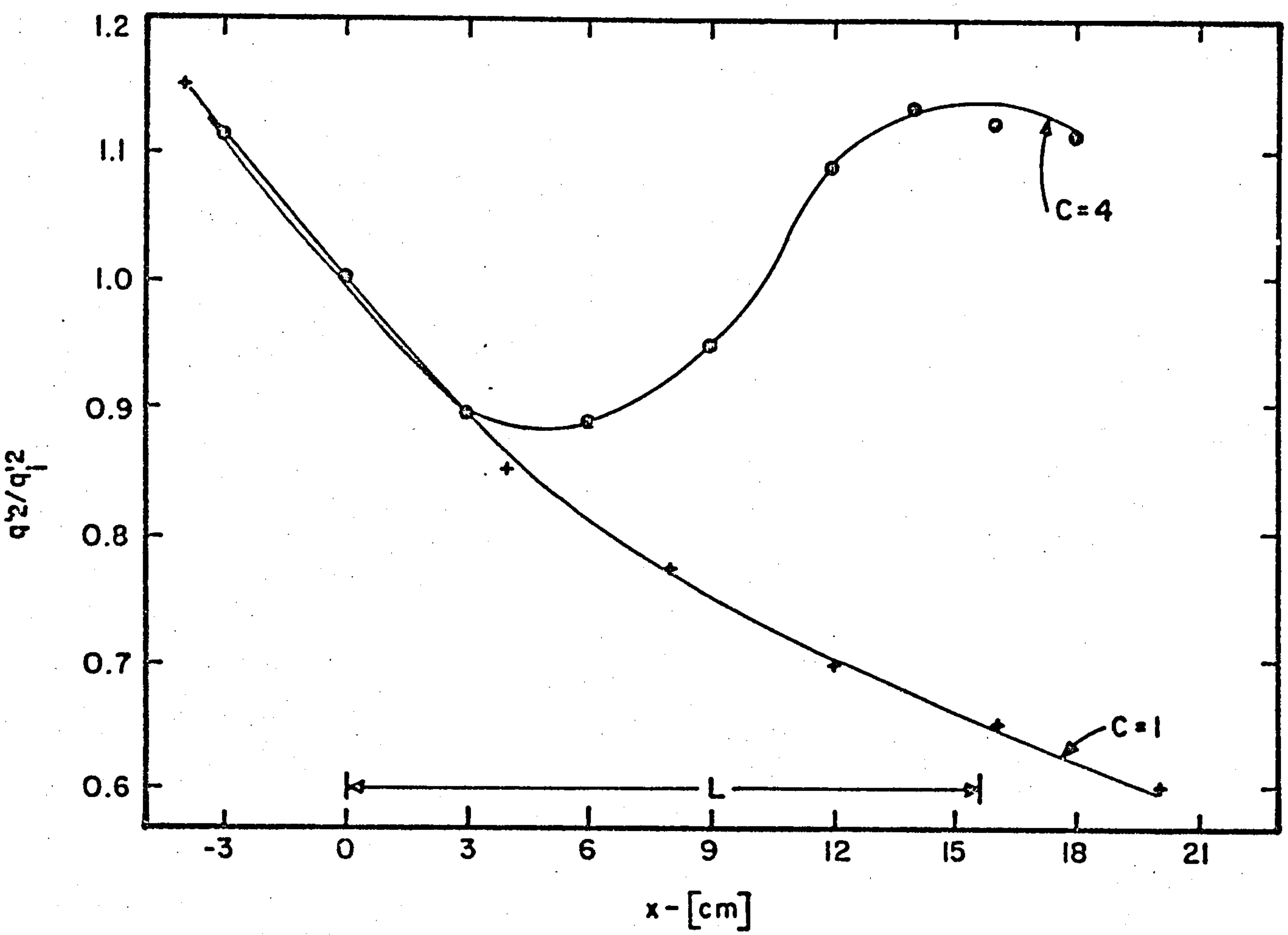

Figure 5. Total Kinetic Energy Along Centerline

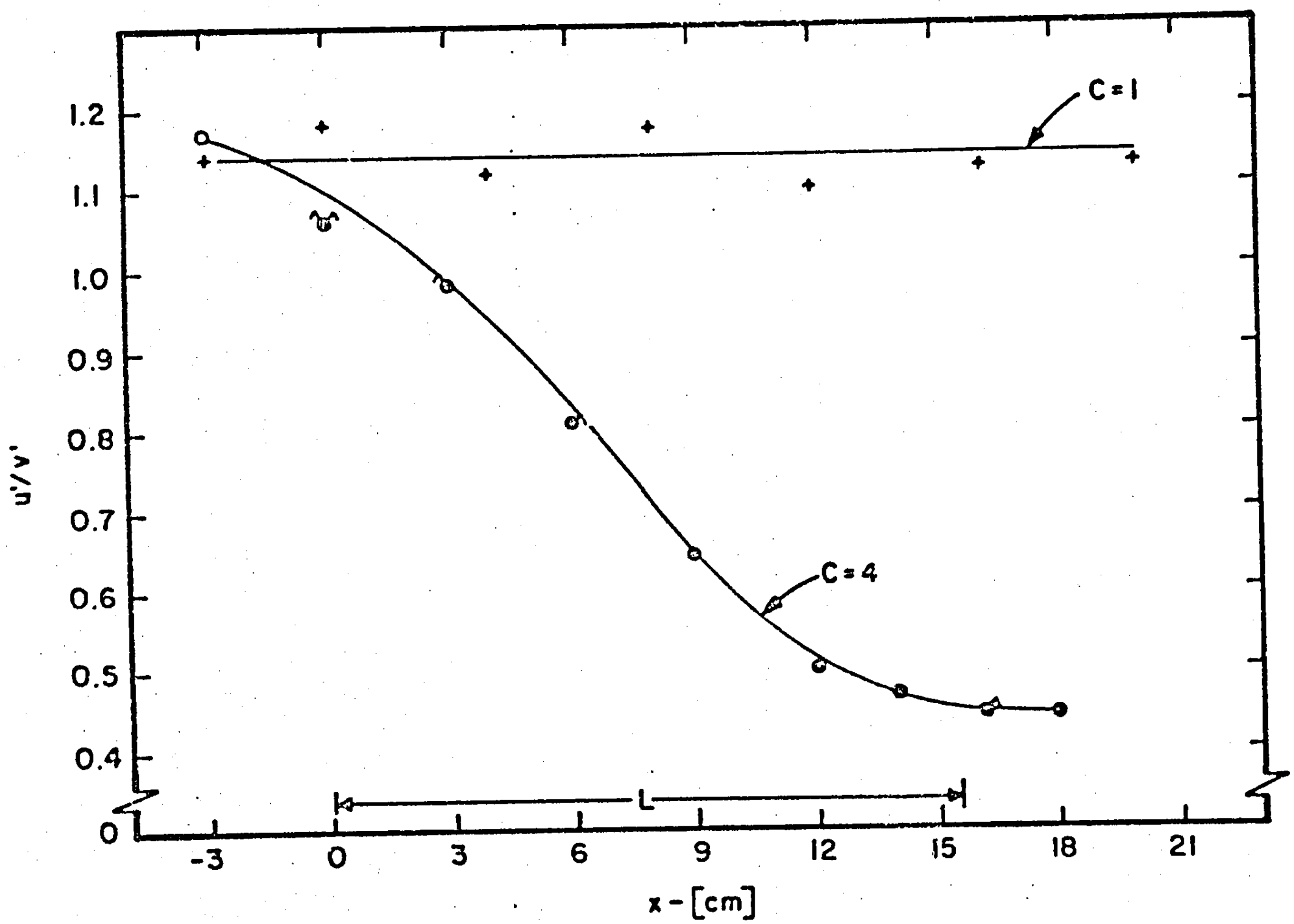

Figure 6. Anisotropy Along Centerline

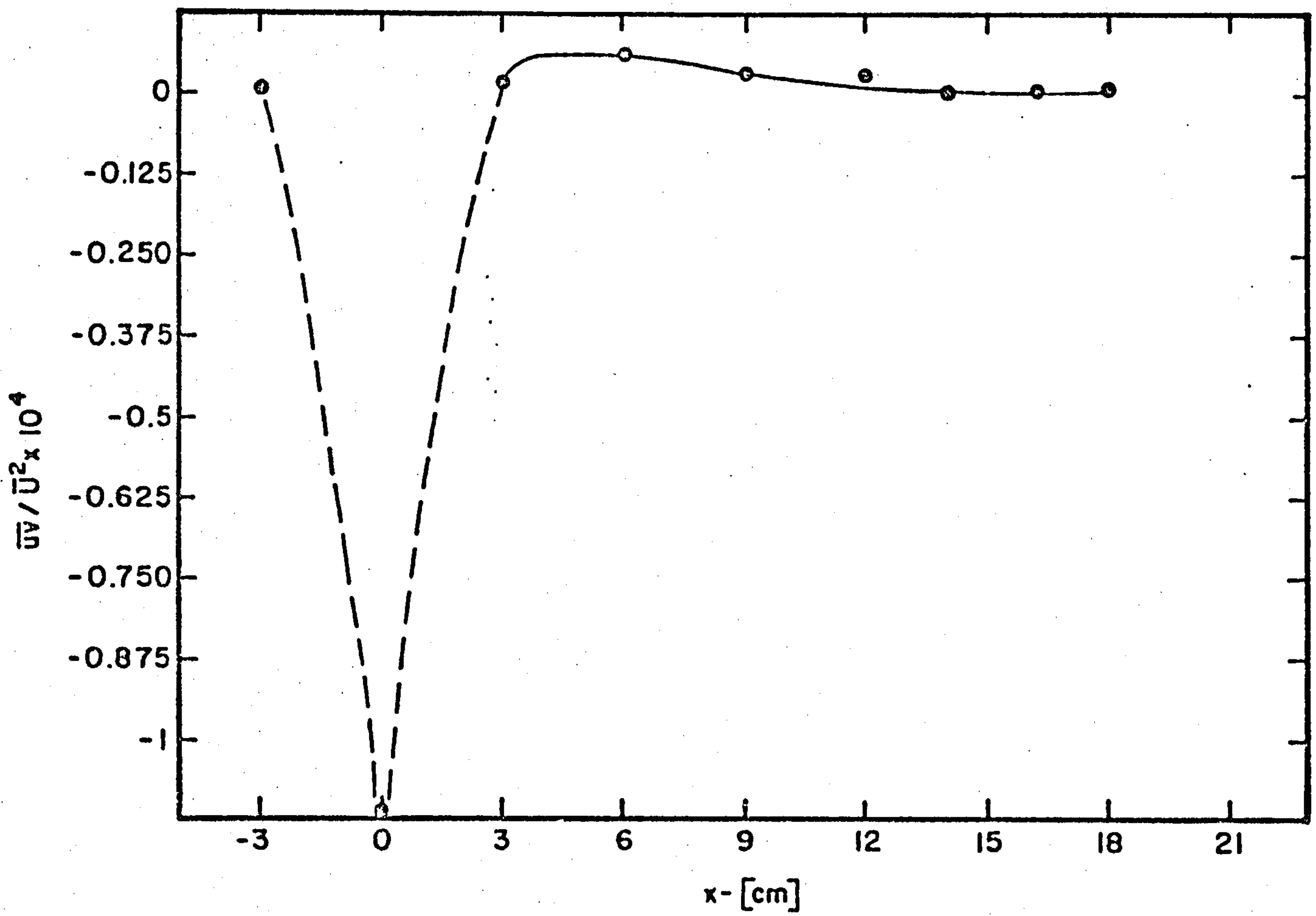

Figure 7. Reynolds Stress Along Centerline

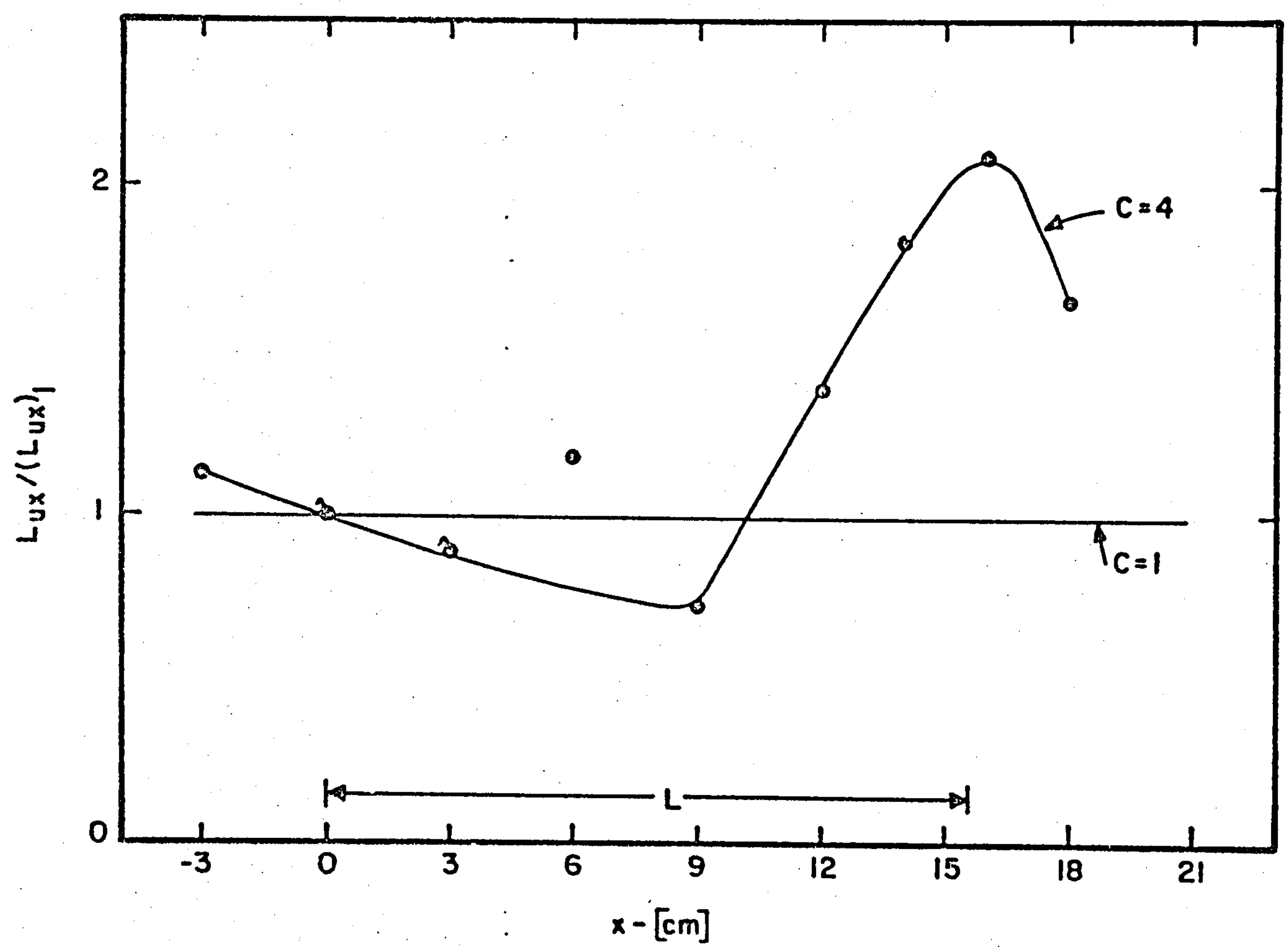

Figure 8. Streamwise Integral Length Scale Based on Longitudinal Velocity Component Along Centerline

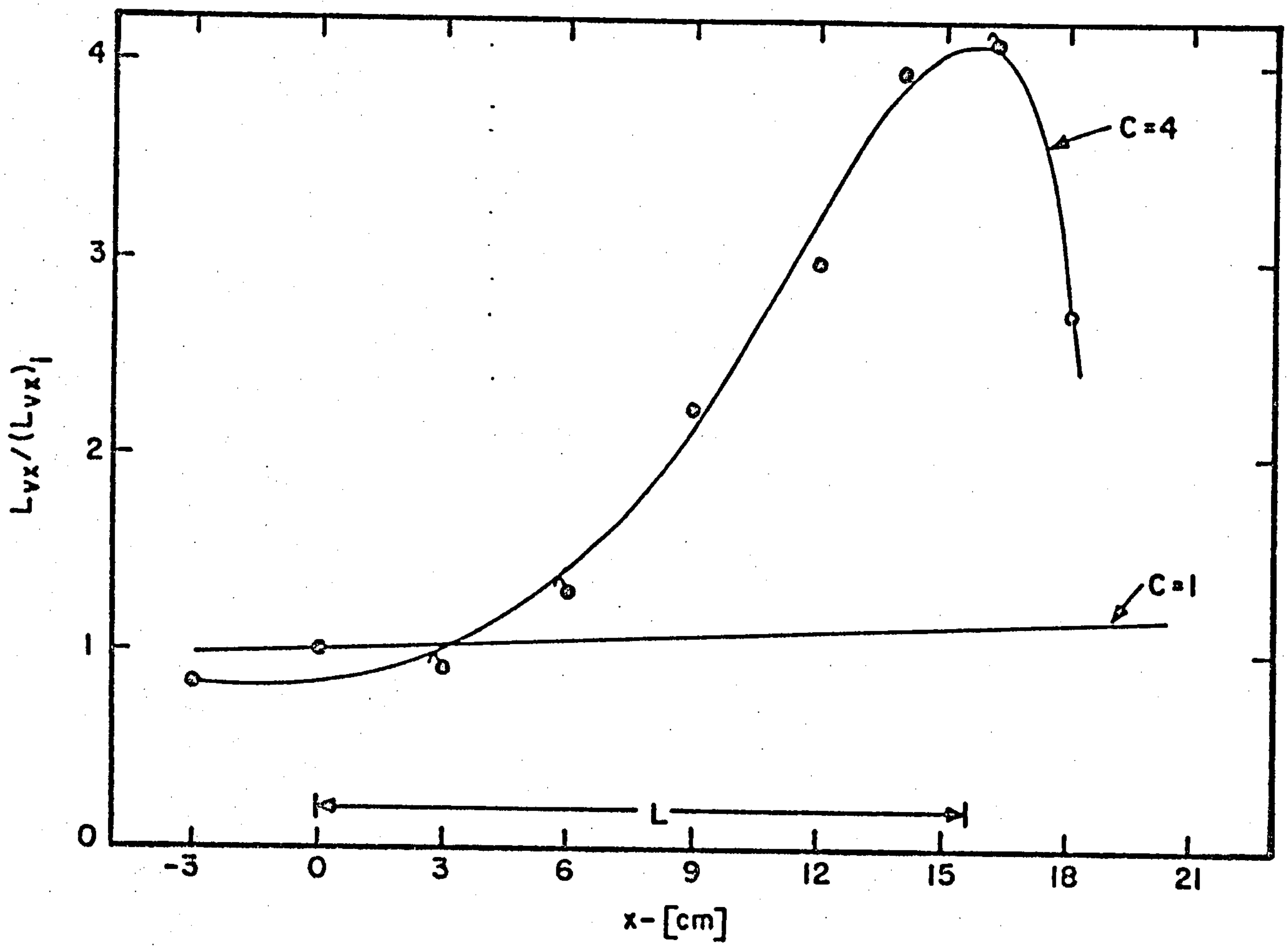

Figure 9. Streamwise Integral Length Scale Based on Lateral Velocity Component Along Centerline

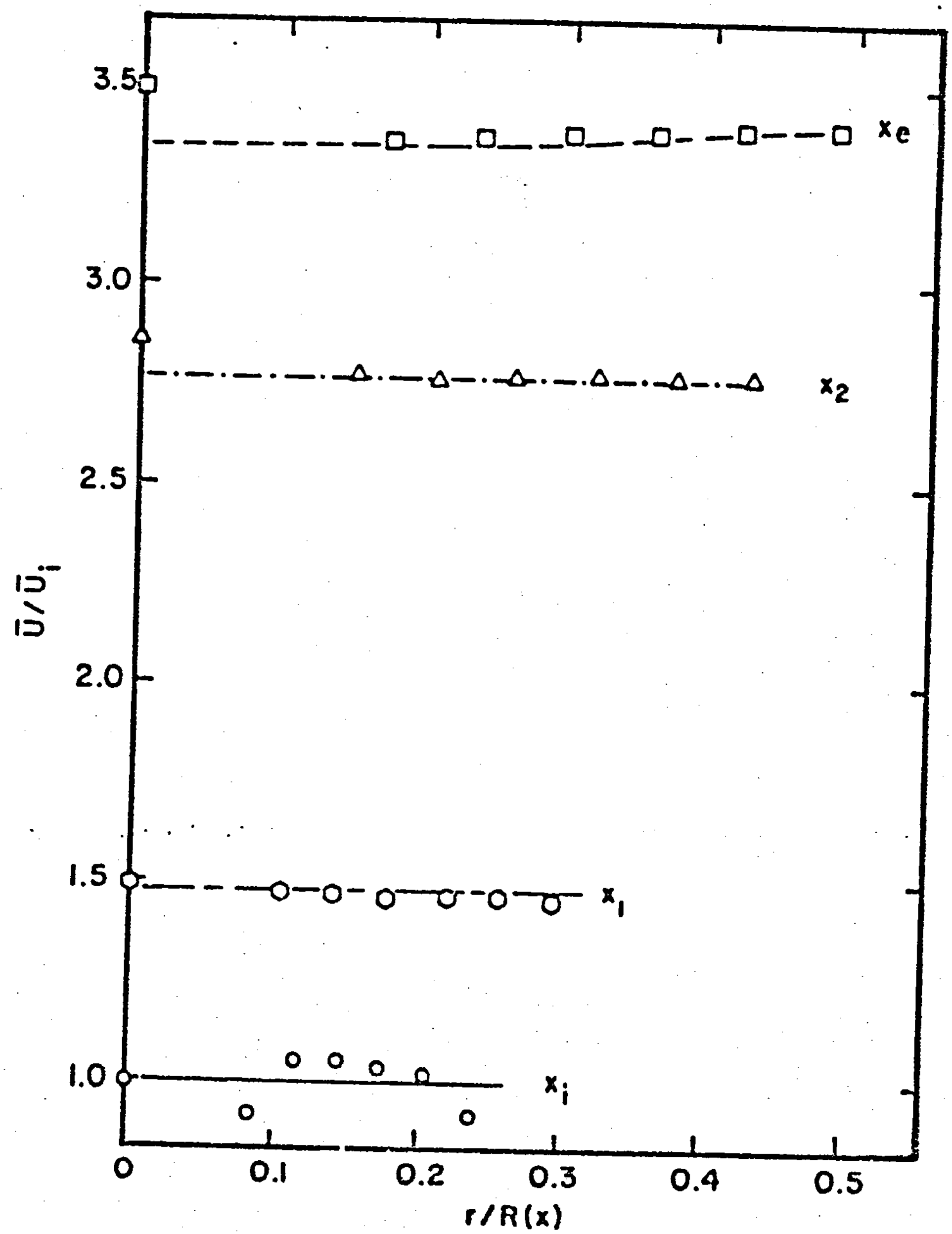

Figure 10. Radial Distribution of Streamwise Mean Velocity at Four Streamwise Locations

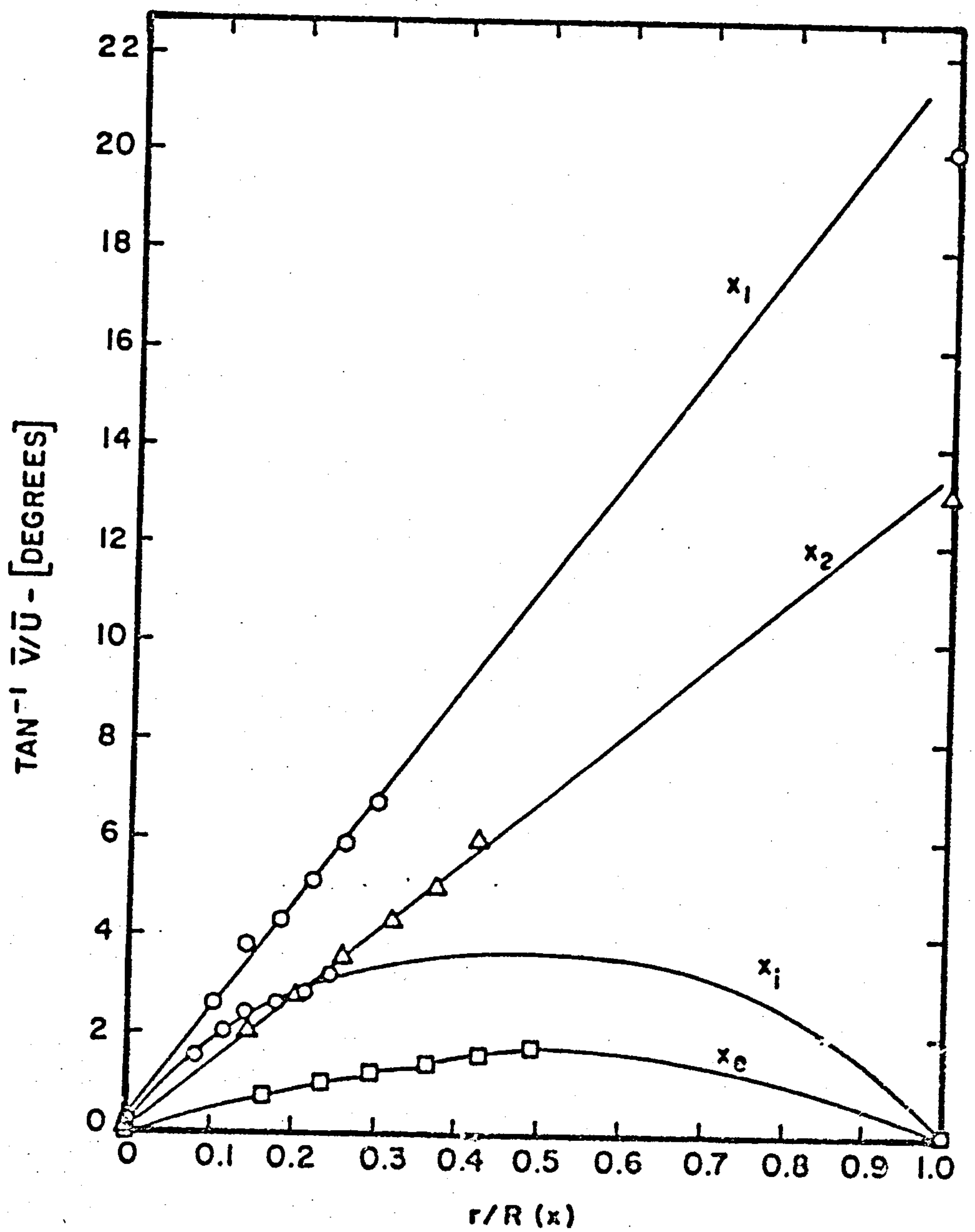

Figure 11. Radial Distribution of Angle of Mean Streamlines at Four Streamwise Locations

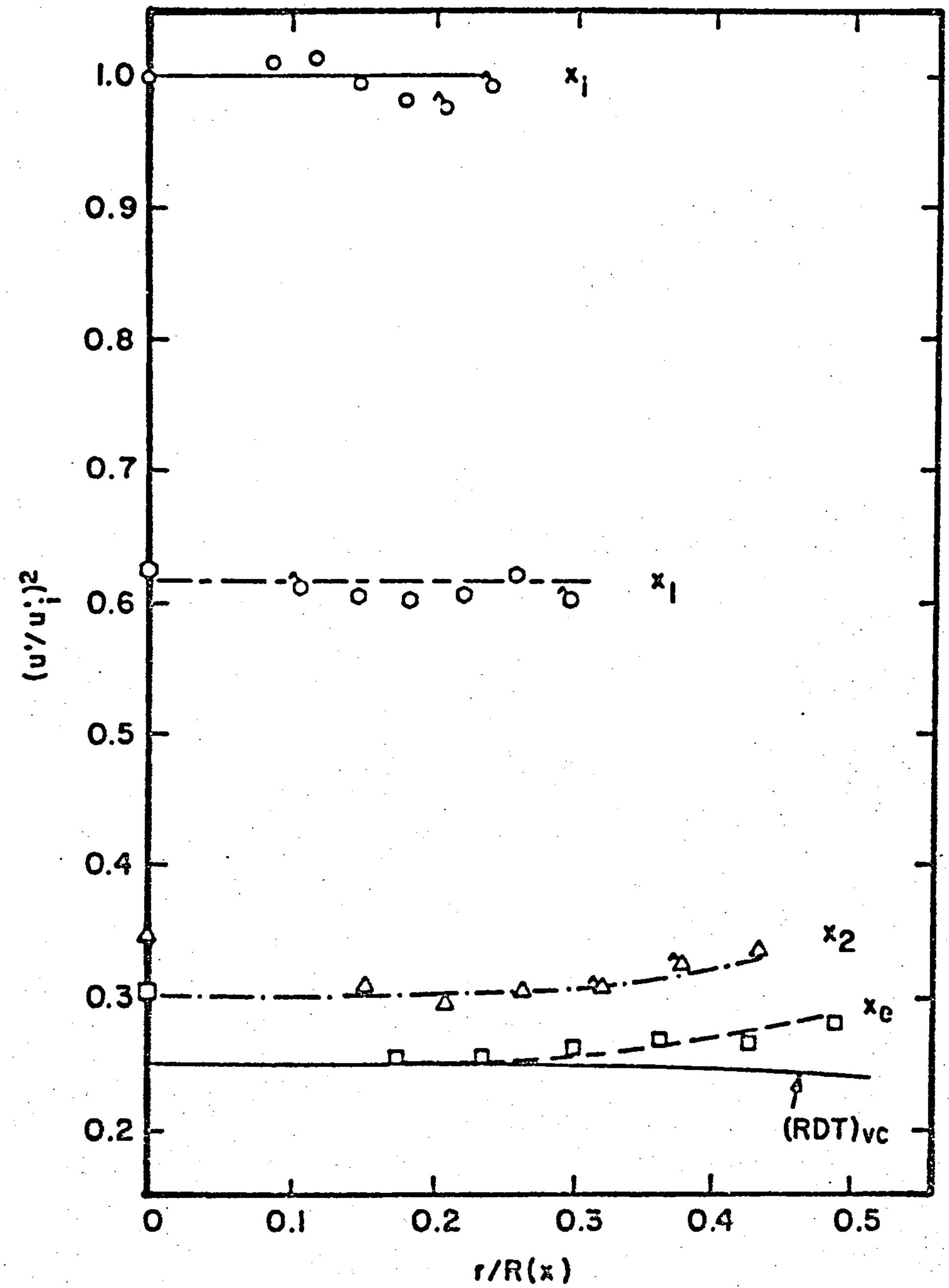

Figure 12. Radial Distribution of Streamwise Kinetic Energy at Four Streamwise Locations

ORIGINAL PAGE IS
OF POOR QUALITY

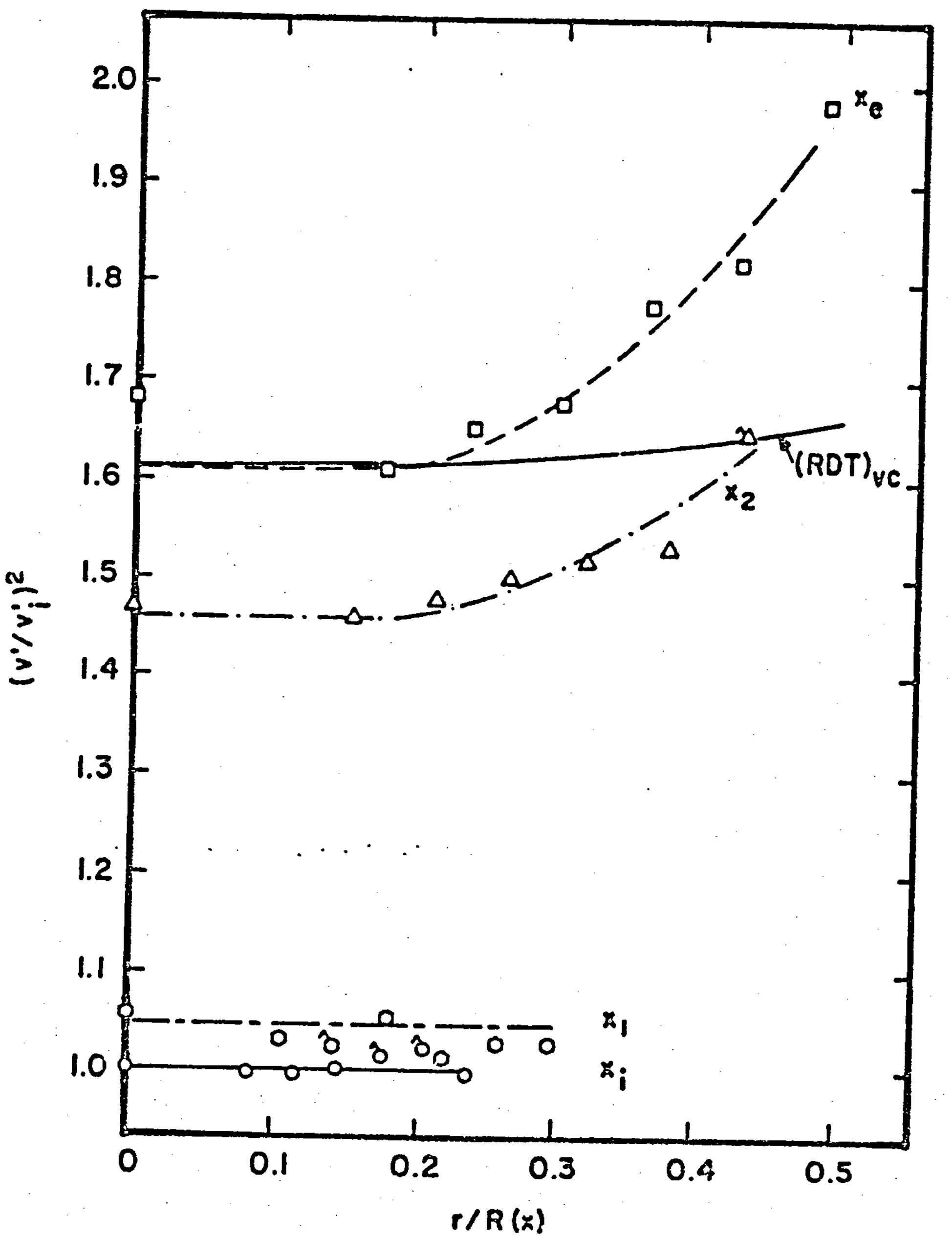

Figure 13. Radial Distribution of Lateral Kinetic Energy at Four Streamwise Locations

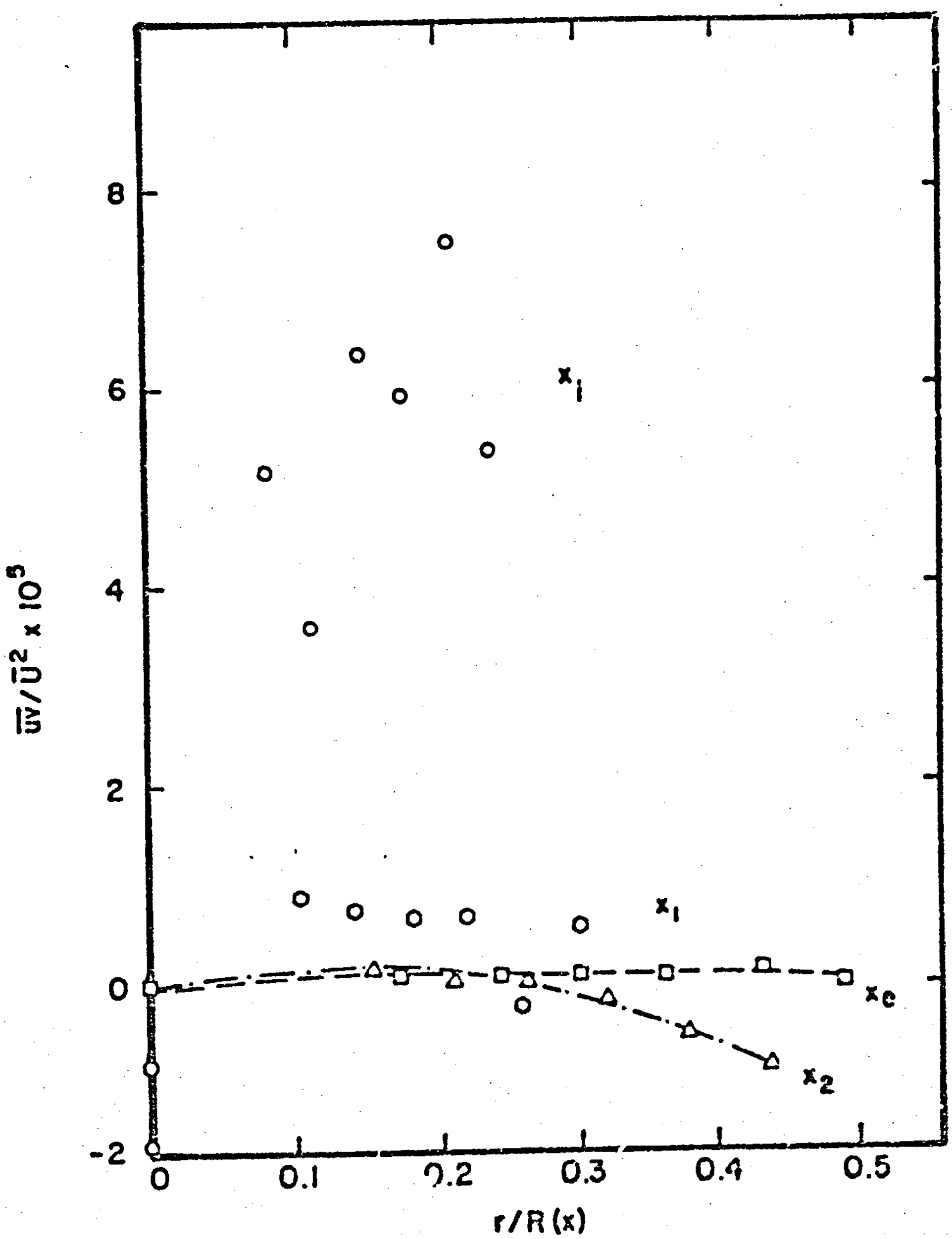

Figure 14. Radial Distribution of Reynolds Stresses at Four Streamwise Locations

ORIGINAL PAGE IS
OF POOR QUALITY

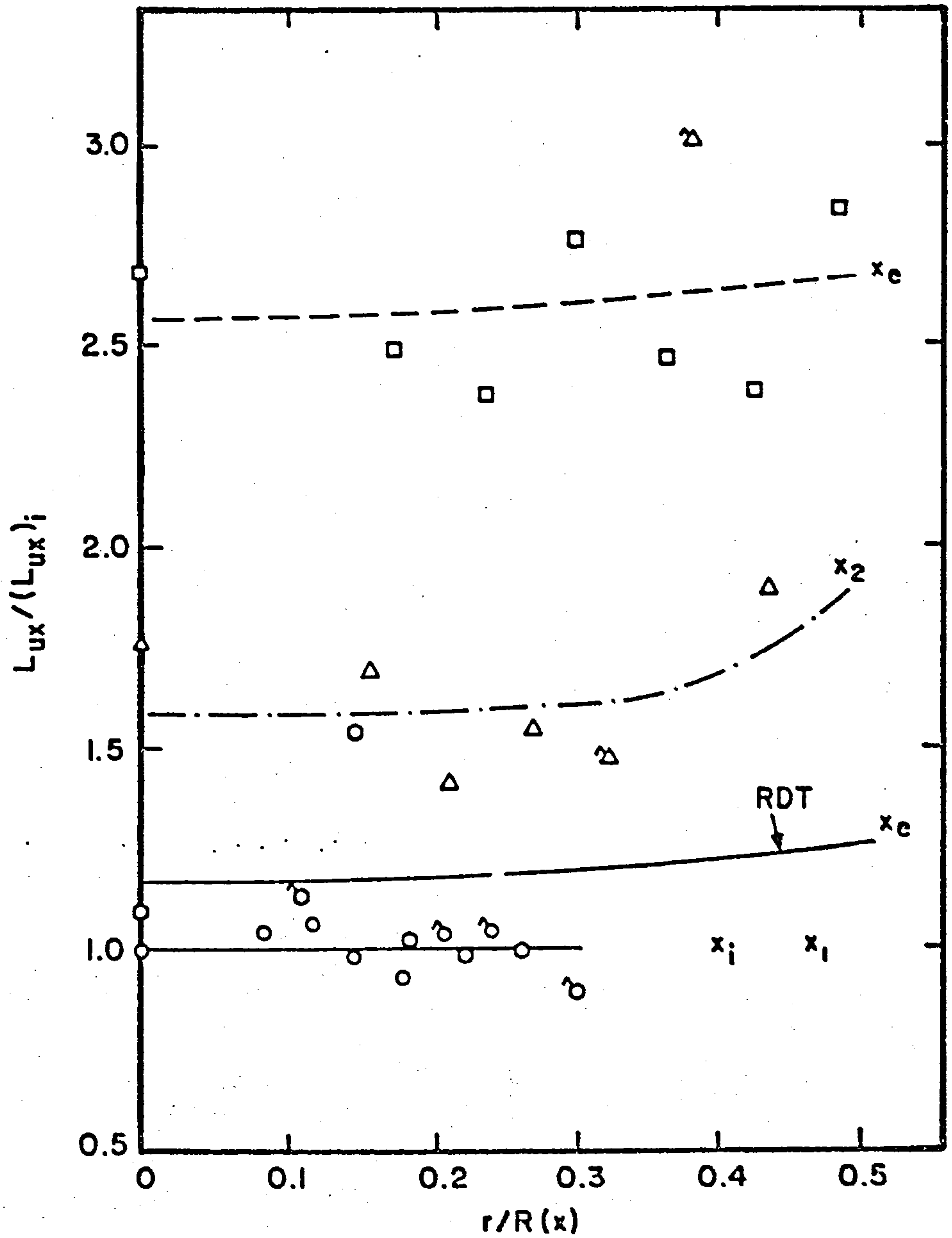

Figure 15. Radial Distribution of Longitudinal Integral Length Scale Based on Streamwise Velocity Component at Four Streamwise Locations

ORIGINAL PAGE IS
OF POOR QUALITY

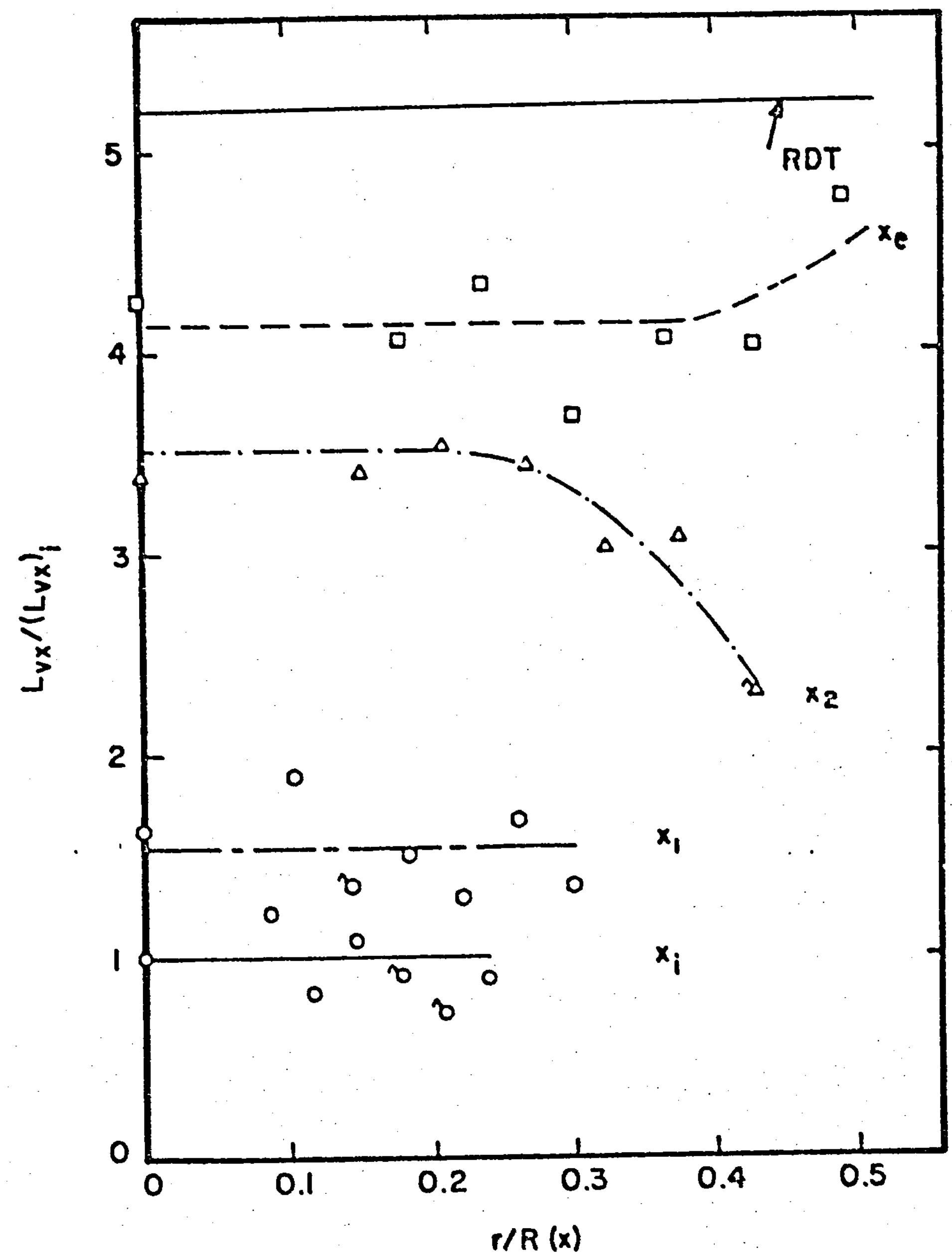

Figure 16. Radial Distribution of Longitudinal Integral Length Scale Based on Lateral Velocity Component at Four Streamwise Locations

ORIGINAL PAGE IS
OF POOR QUALITY

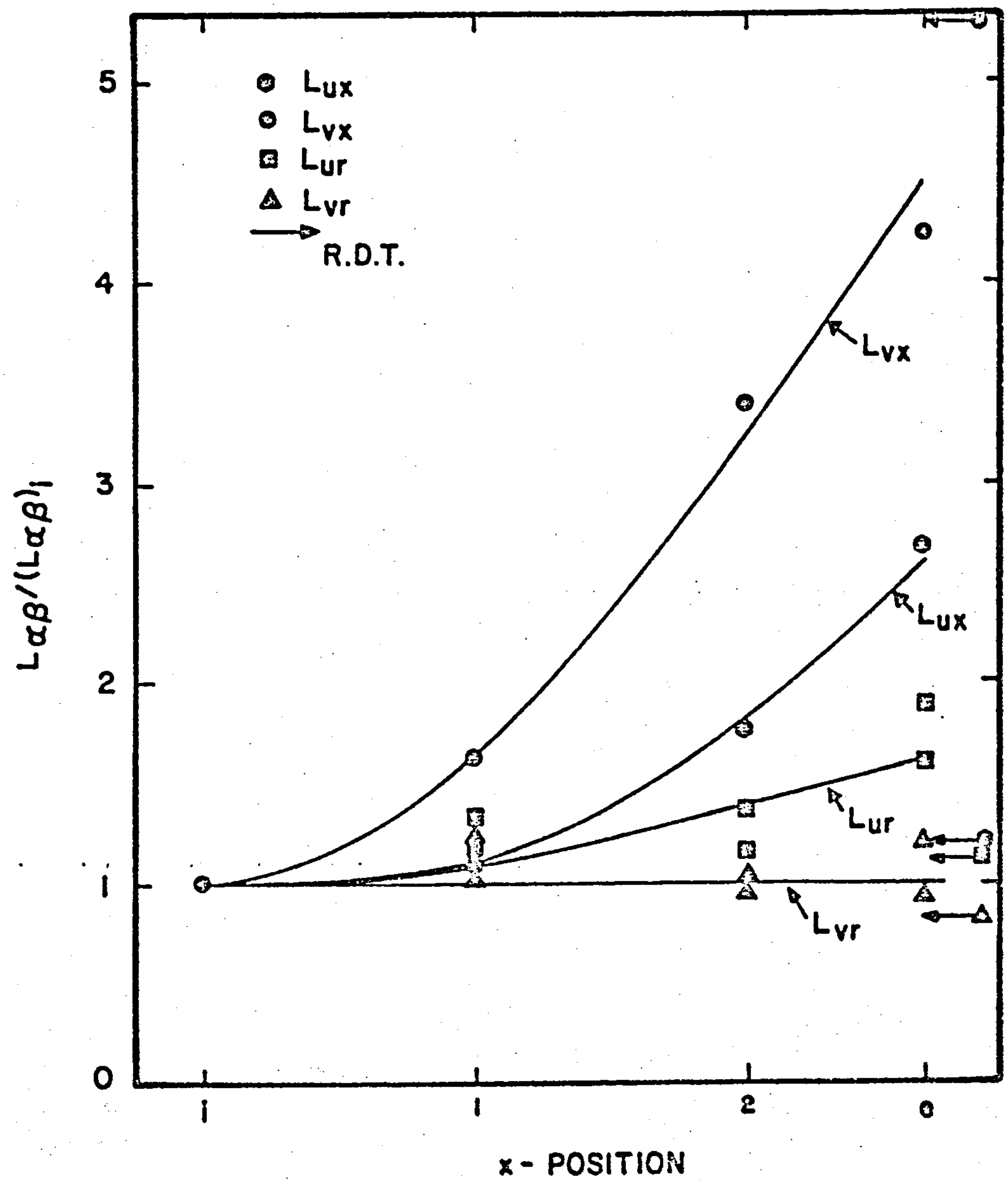

Figure 17. Streamwise Evolution of Integral Length Scales Normalized by Their Respective Values at the Inlet

ORIGINAL PAGE IS
OF POOR QUALITY

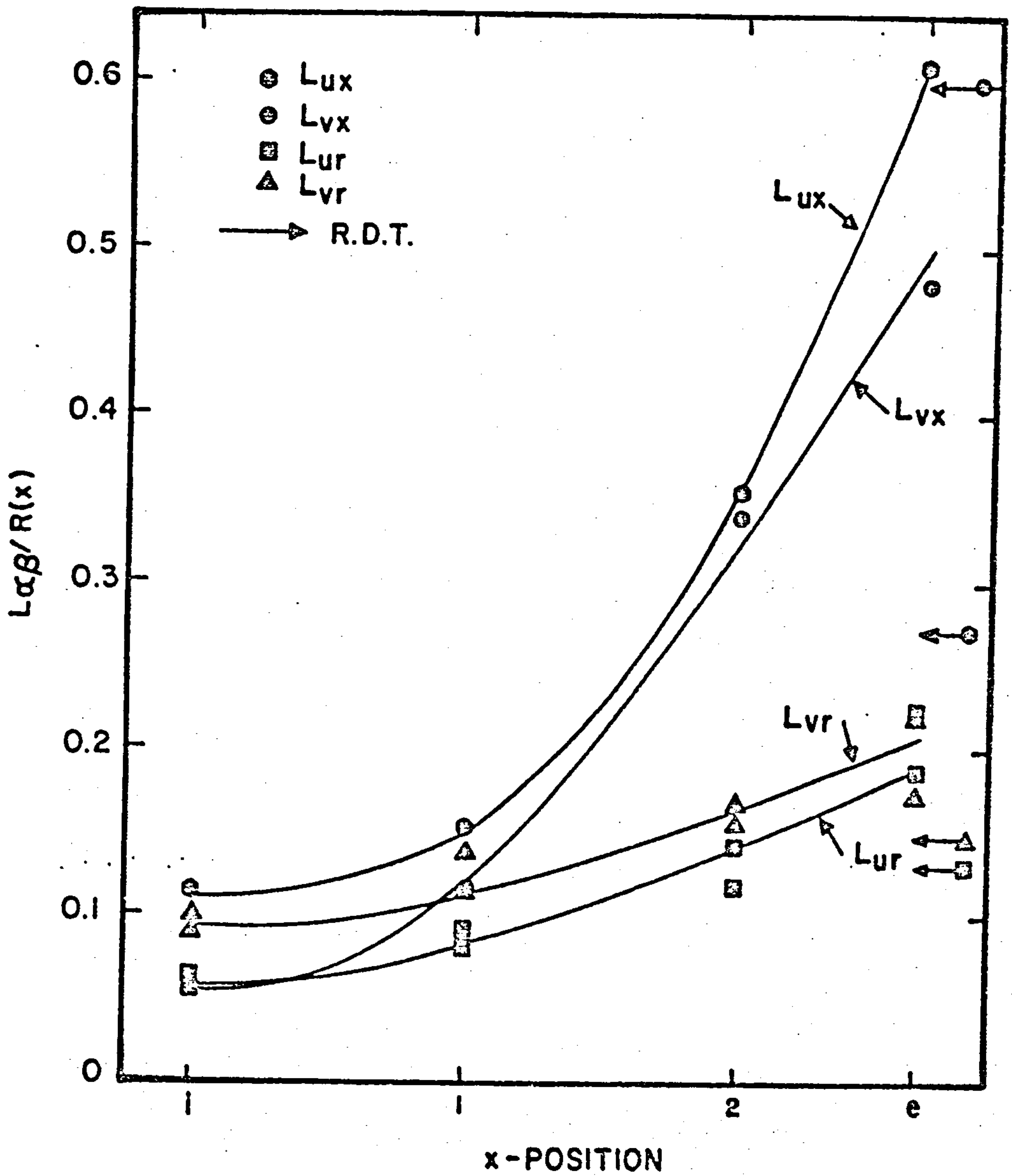

Figure 18. Streamwise Evolution of Integral Length Scales Normalized by Local Radius of Contraction

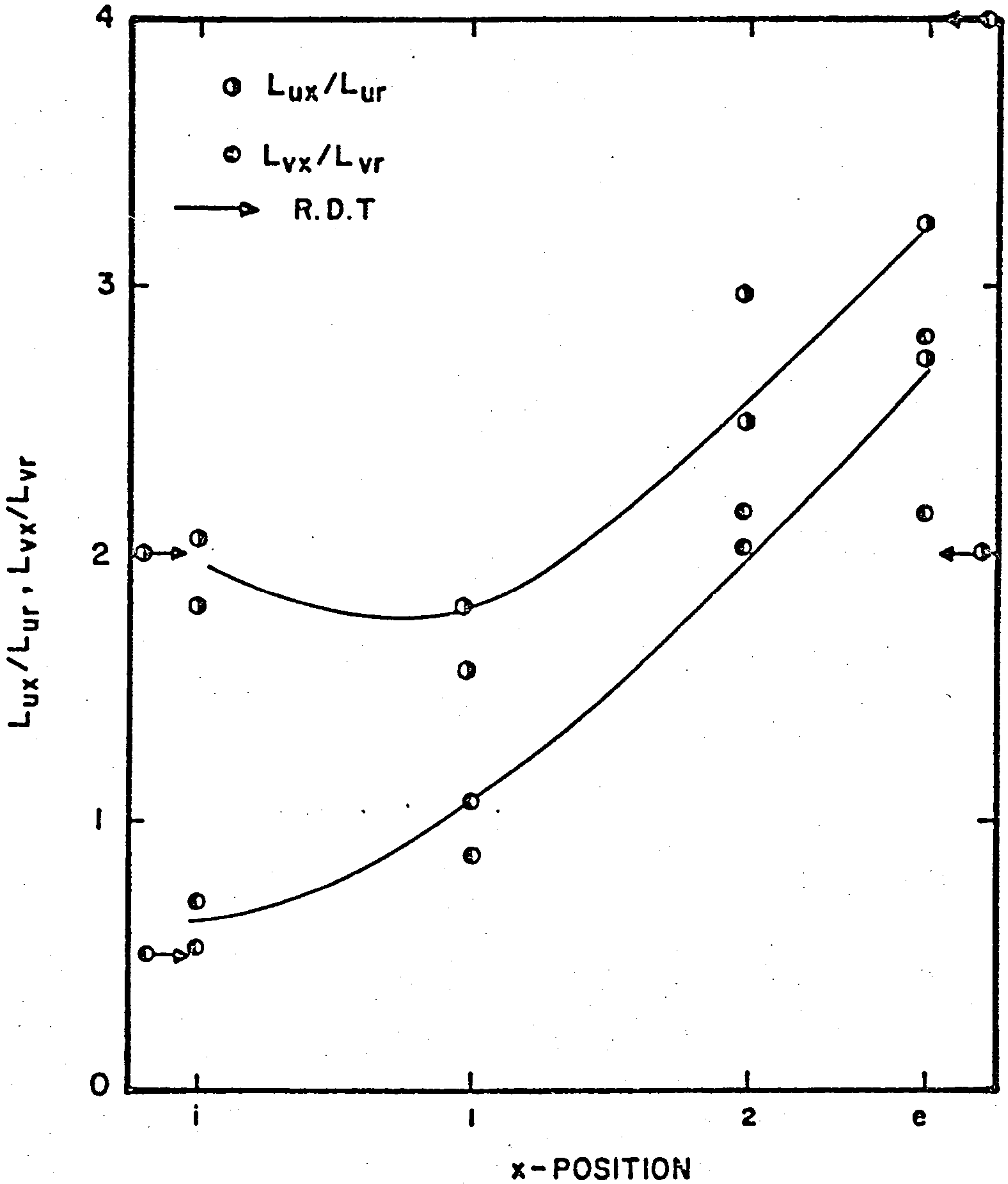

Figure 19. Streamwise Evolution of Length-Scale Aspect Ratios for Both Velocity Components

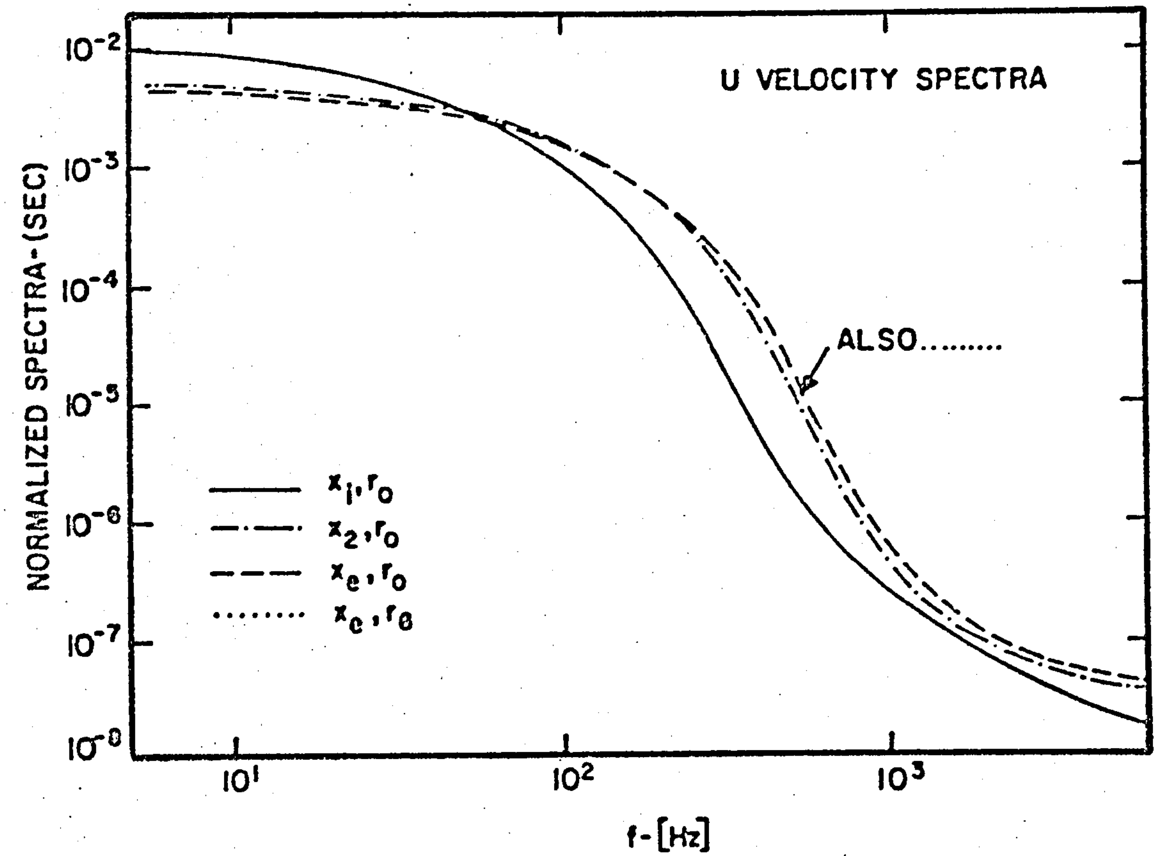

Figure 20. Evolution of Normalized Spectra of Streamwise Velocity

ORIGINAL PAGE IS
OF POOR QUALITY

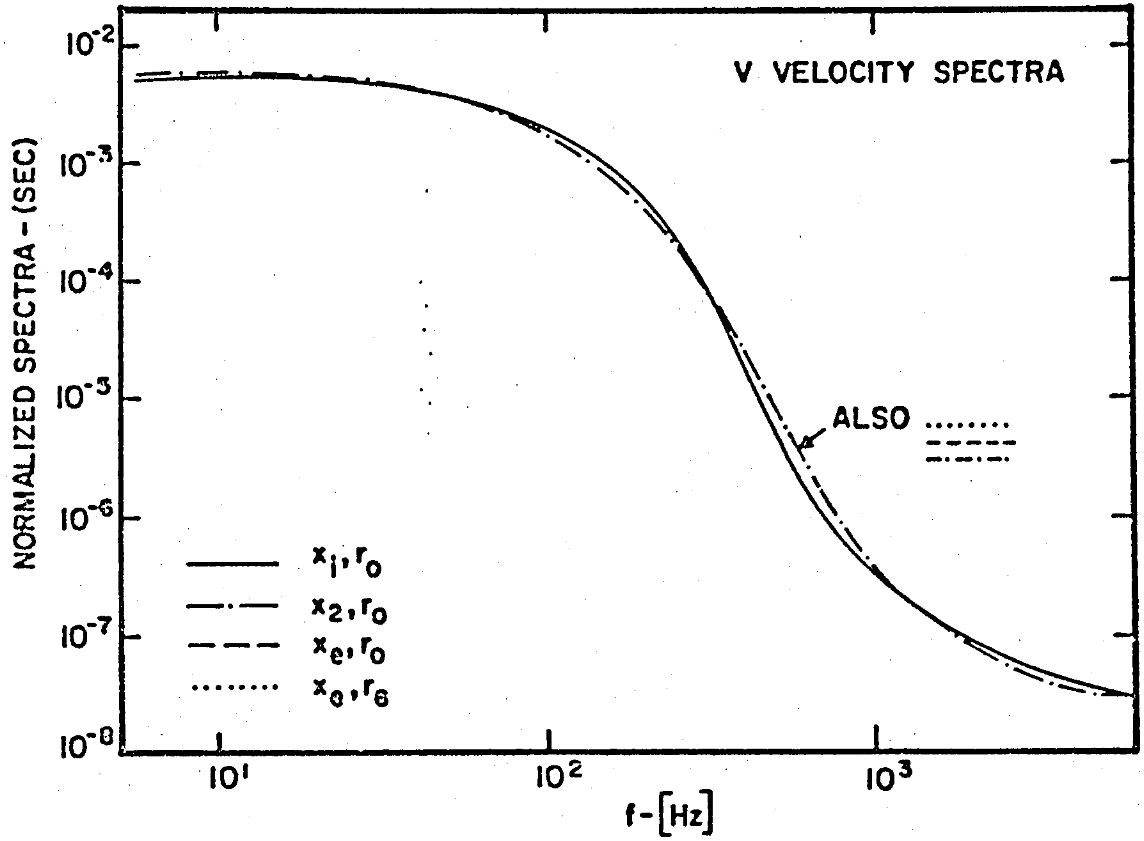

Figure 21. Evolution of Normalized Spectra of Transverse Velocity

ORIGINAL PAGE IS OF POOR QUALITY

ORIGINAL PAGE IS
OF POOR QUALITY

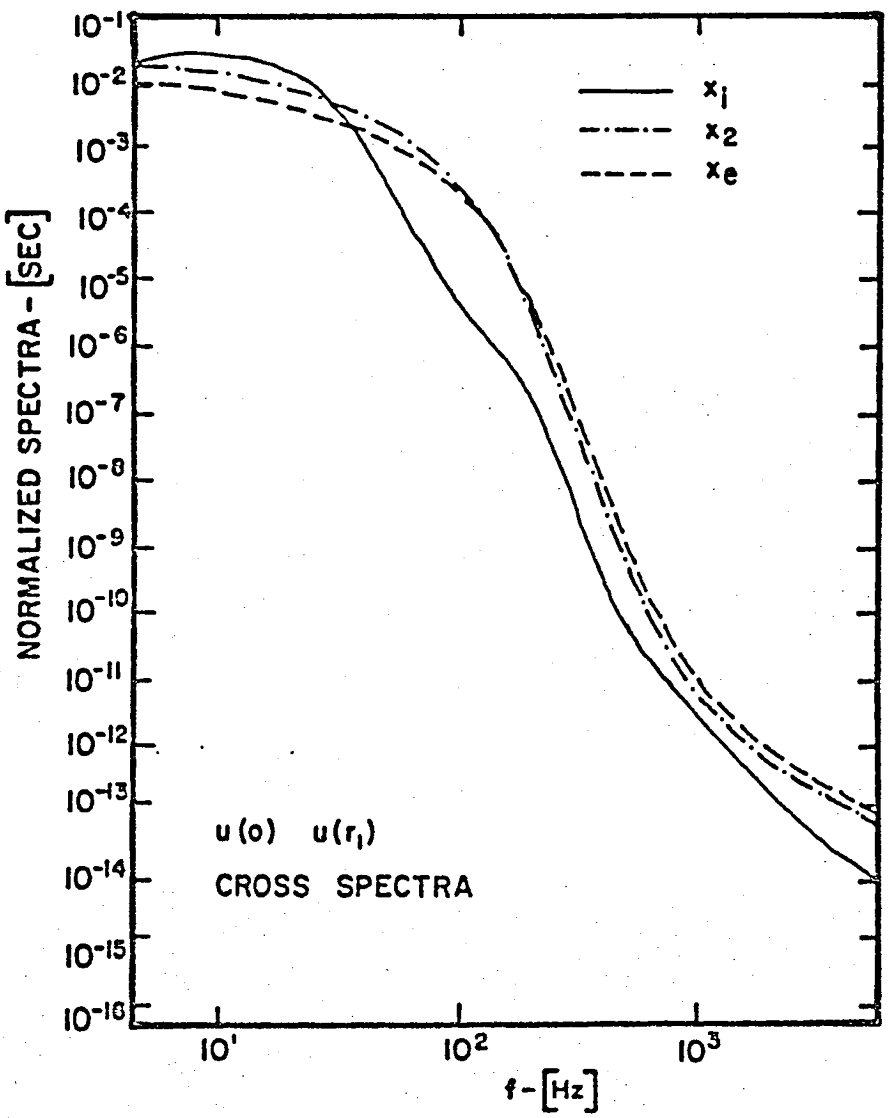

Figure 22. Evolution of Normalized Cross-Spectra of Streamwise Velocities

ORIGINAL PAGE IS
OF POOR QUALITY

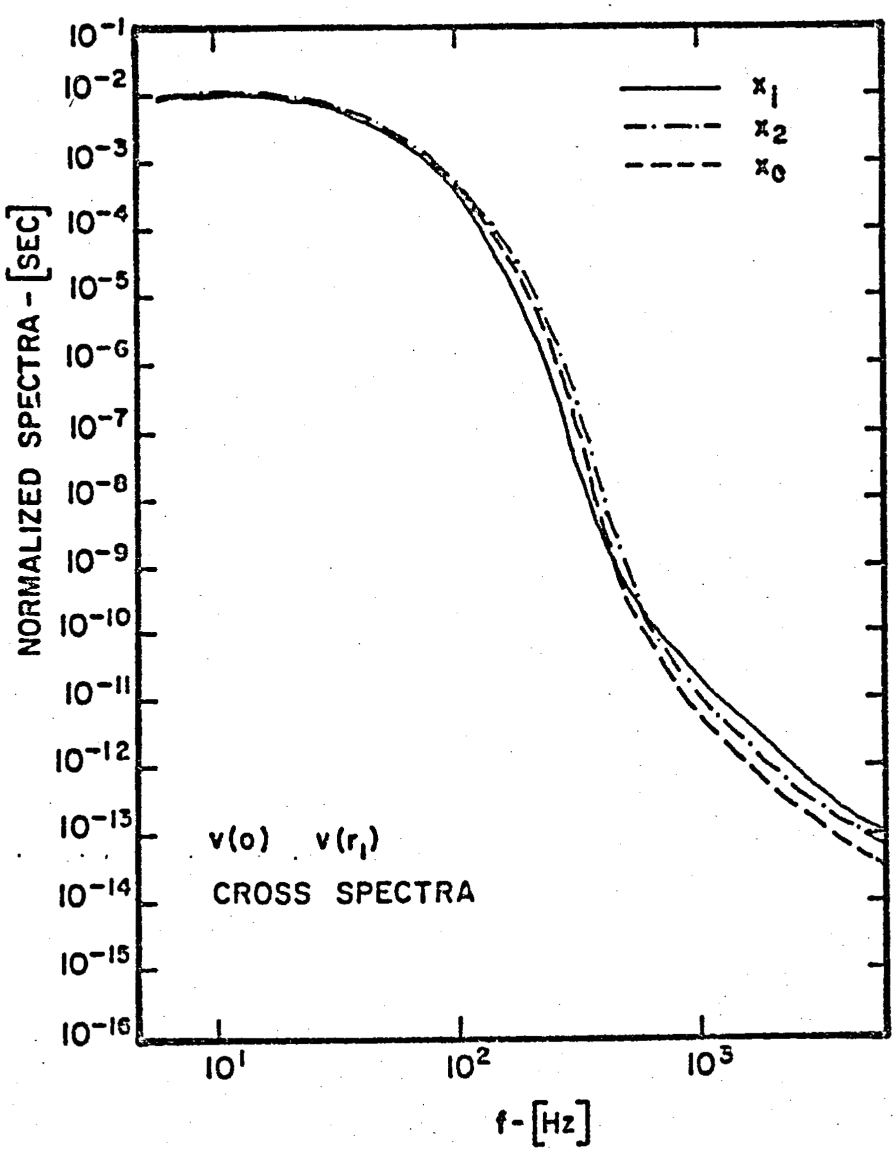

Figure 23. Evolution of Normalized Cross-Spectra of Transverse Velocities

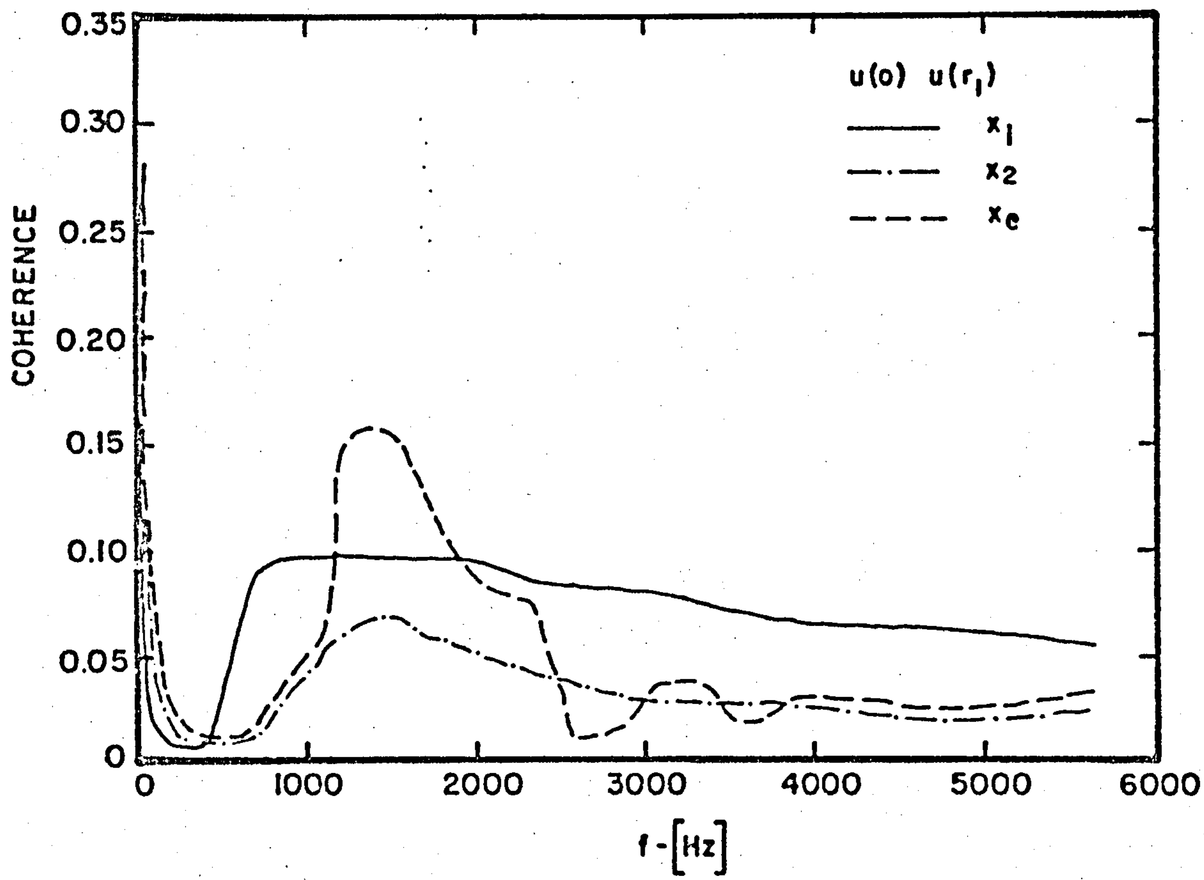

Figure 24. Evolution of Cross-Coherence of Streamwise Velocities for Probe Separation Comparable to Length Scales

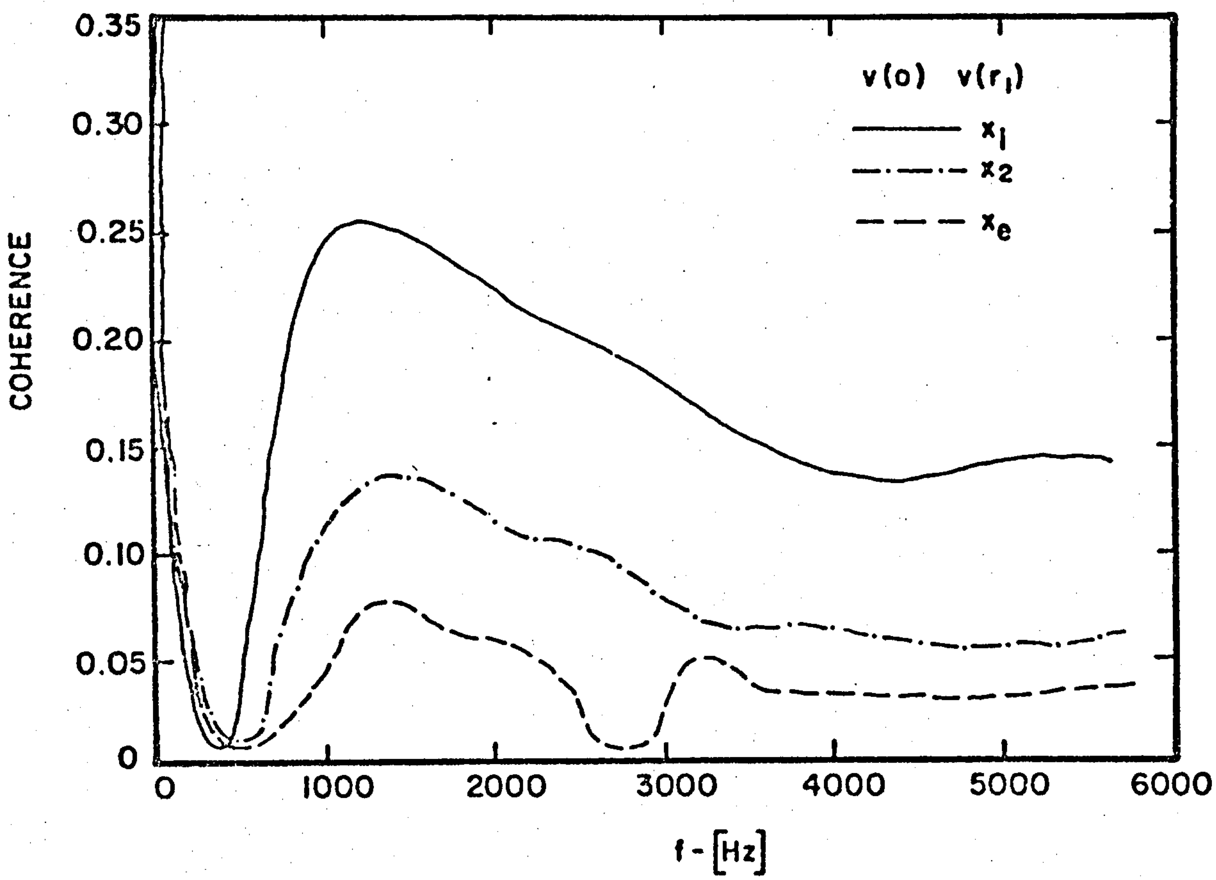

Figure 25. Evolution of Cross-Coherence of Streamwise Velocities for Probe Separation Larger Than Length Scales

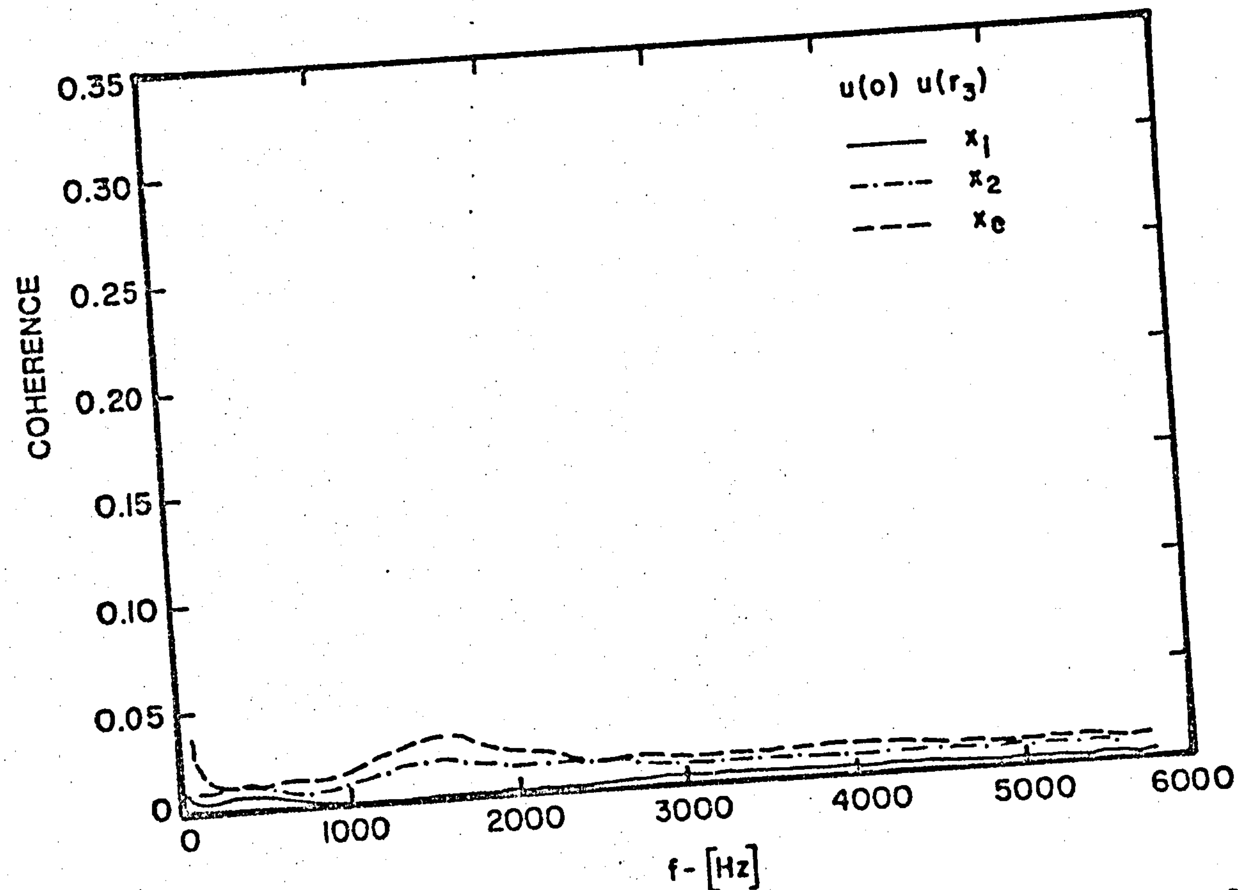

Figure 26. Evolution of Cross-Coherence of Streamwise Velocities for Probe Separation Much Larger Than Length Scales

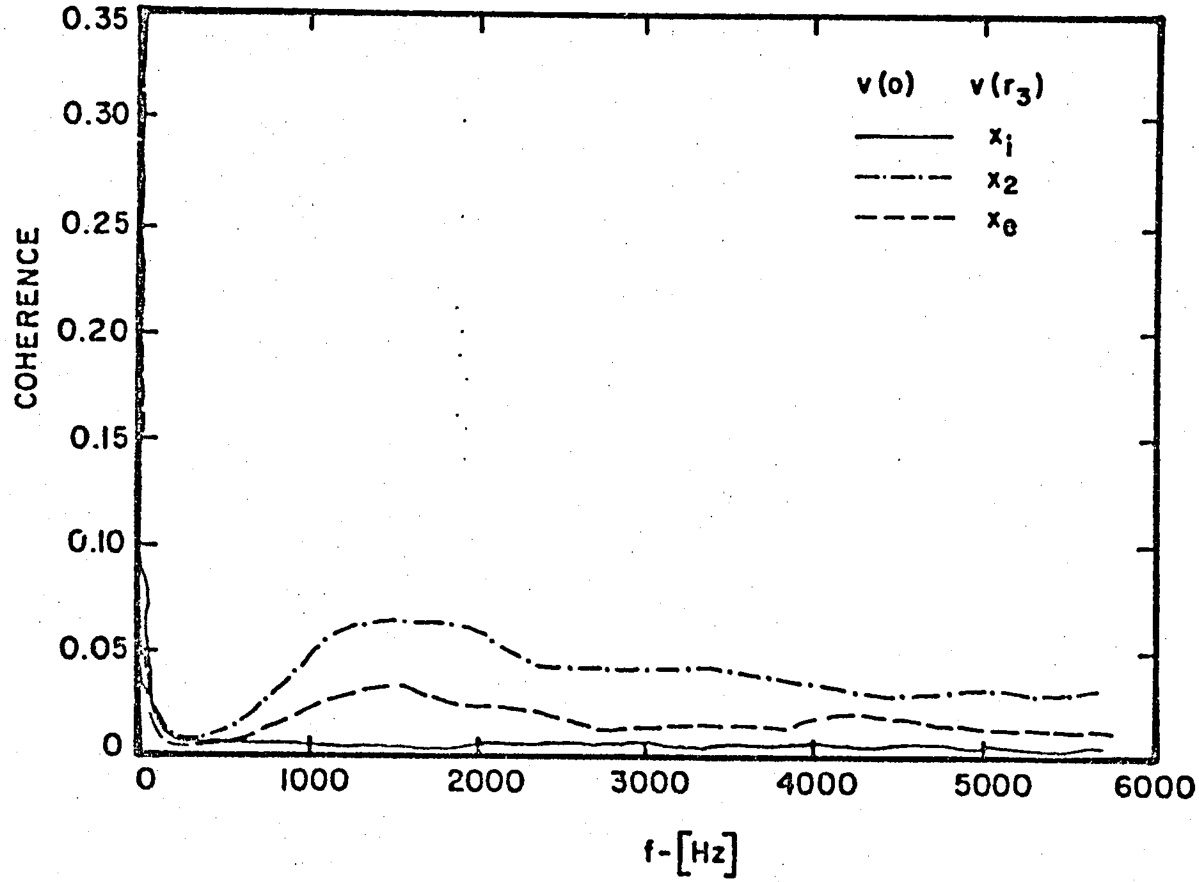

ORIGINAL PAGE IS OF POOR QUALITY

Figure 27. Evolution of Cross-Coherence of Transverse Velocities for Probe Separation Comparable to Length Scales

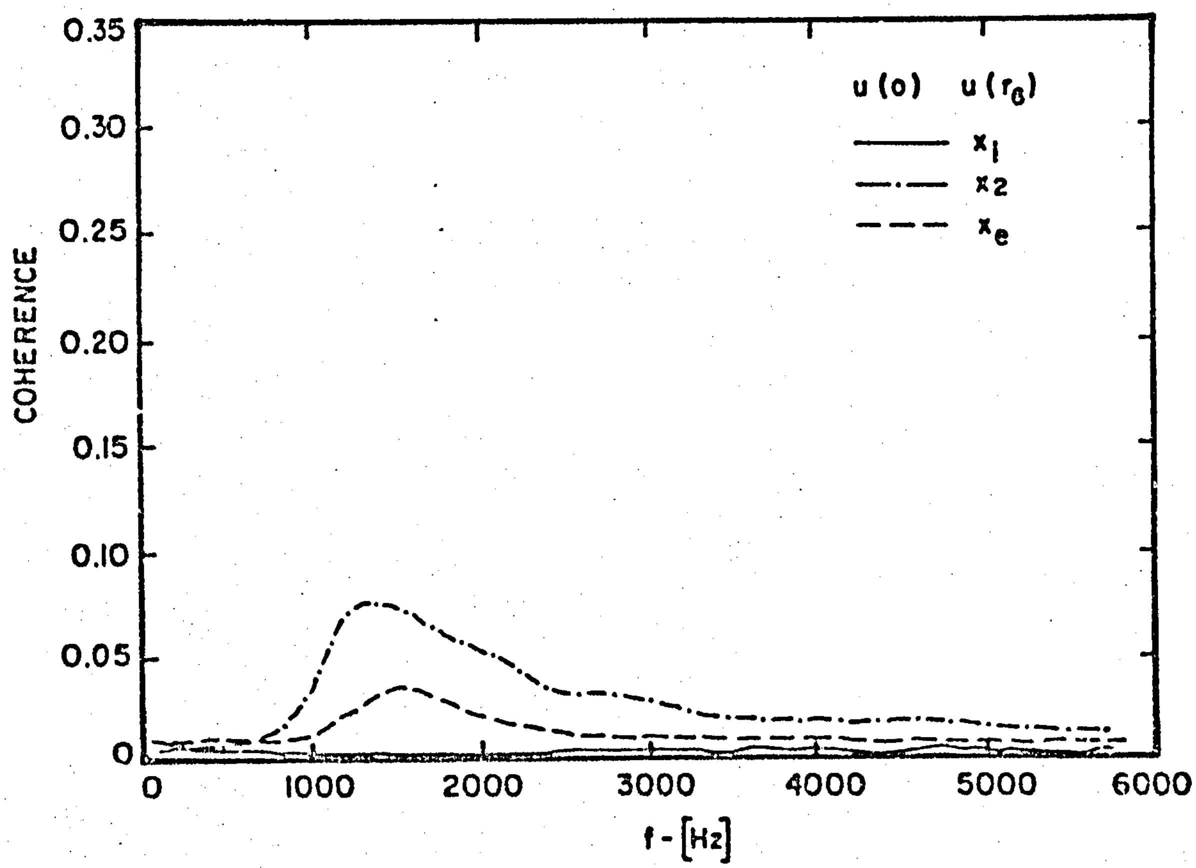

Figure 28. Evolution of Cross-Coherence of Transverse Velocities for Probe Separation Larger Than Length Scales

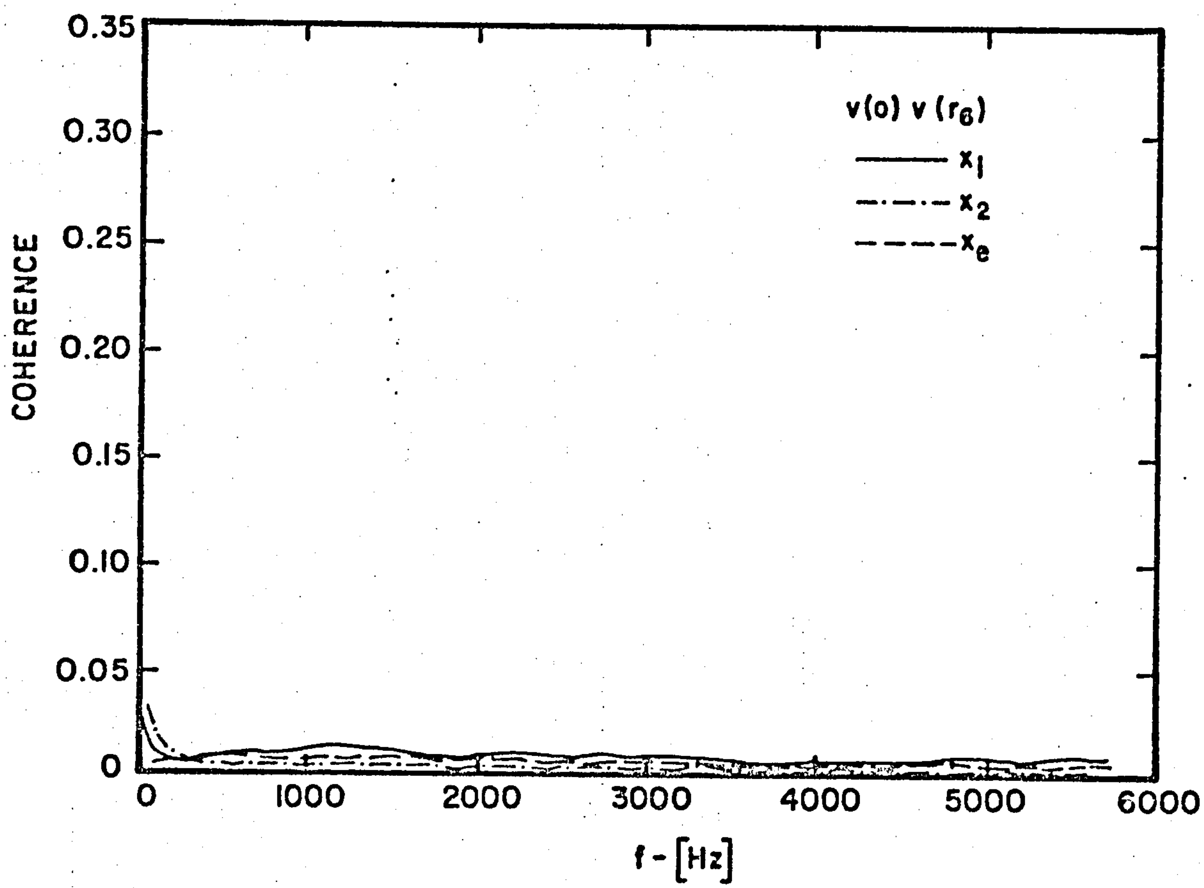

Figure 29. Evolution of Cross-Coherence of Transverse Velocities for Probe Separation Much Larger Than Length Scales

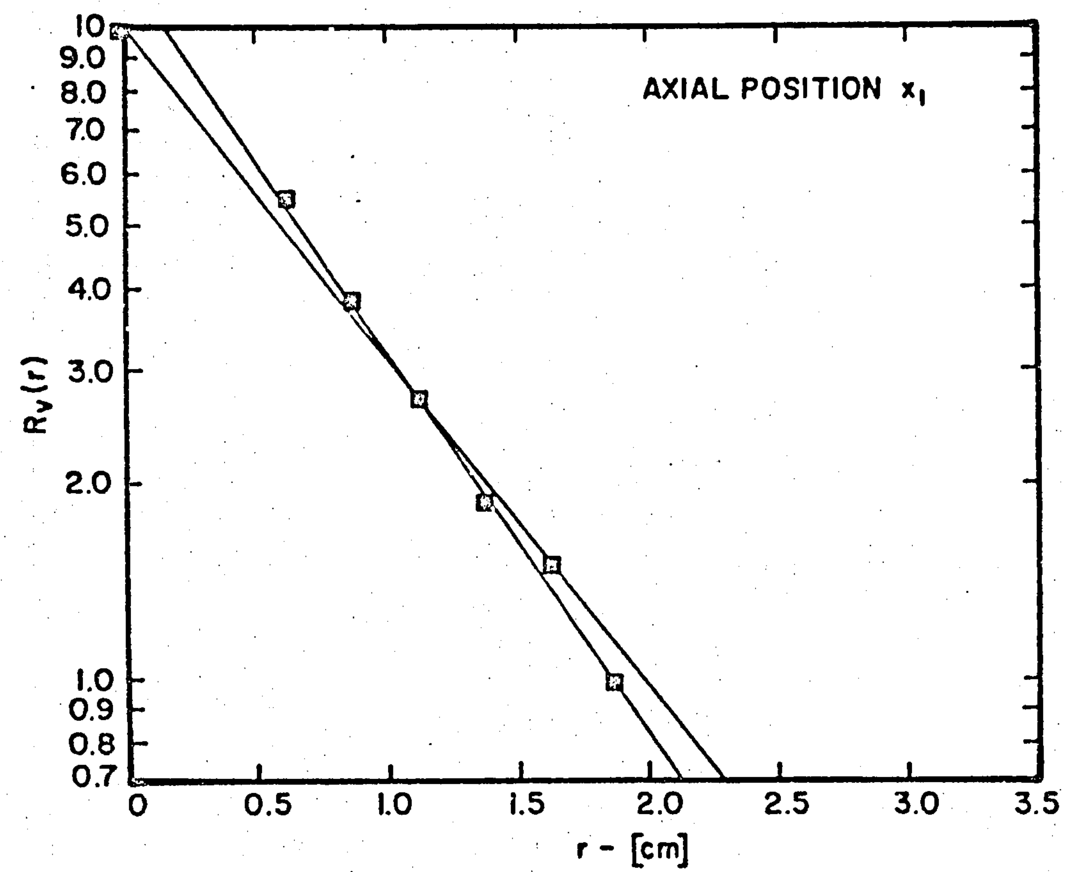

Figure 30. Sample of Velocity-Correlation Plots Used to Calculate Lateral Integral Length Scales

BIBLIOGRAPHY

Batchelor, G. K. and Proudman, L. 1954. The Effect of Rapid Distortion of a Fluid in Turbulent Motion. J. Mech. Appl. Math. 7, 83-101.

Batchelor, G. K. 1956. The Theory of Homogeneous Turbulence, Cambridge University Press, Cambridge.

Chen, S. C. 1981. The Distortion of Turbulence by an Axisymmetric Contracting Flow. M.S. Thesis, Department of Mechanics and Mechanical and Aerospace Engineering, Illinois Institute of Technology.

Drubka, R. E. and Wlezien, R. W. 1979. Efficient Velocity Calibration and Yaw-Relation Truncation Errors in Hot-Wire Measurements of Turbulence. Abstract published in the Bulletin of the American Physical Society, Fluid Dynamics Division, Vol. 24, 1979, 1142.

Goldstein, M. E. 1978. Unsteady Vortical and Entropic Distortions of Potential Flows Around Arbitrary Obstacles. J. Fluid Mech. 89, 633-668.

Goldstein, M. E. 1979. Turbulence Generated by the Interaction of Entropy Fluctuations With Nonuniform Mean Flows. J. Fluid Mech., Vol. 93, 209-224.

Hanson, D. B. 1977. Study of Noise and Inflow Distortion Sources in the NASA QF-1B Fan Using Measured Blade and Vane Pressures. NASA Contractor Rept. No. CR-2899.

Hinze, J. O. 1959. Turbulence. 2nd Edition, McGraw-Hill, New York, N.Y.

Hunt, J. C. R. 1973. A Theory of Turbulent Flow Round Two-Dimensional Bluff Bodies. J. Fluid Mech. 61, 625-706.

Loehrke, R. I. and Nagib, H. M. 1972. Experiments on Management of Free-Stream Turbulence. AGARD Rept. No. 598, DD-749-891.

Marion, A. 1983. On the Design of Contractions and Settling Chambers for Optimal Turbulence Manipulation in Wind Tunnels. M.S. Thesis, Department of Mechanics and Mechanical and Aerospace Engineering, Illinois Institute of Technology.

Ribner, H. S. and Tucker, M. 1953. Spectrum of Turbulence in a Contracting Stream. N.A.C.A. Rept. No. 1113.

Tan-atichat, J. 1980. Effects of Axisymmetric Contractions on Turbulence of Various Scales. Ph.D. Thesis, Department of Mechanics and Mechanical and Aerospace Engineering, Illinois Institute of Technology. (Also available as NASA Contractor Rept. 165136).

Tan-atichat, J., Nagib, H. M. and Loehrke, R. I. 1982. Interaction of Free Stream Turbulence With Screen and Perforated Plates: A Balance Between Turbulent Scales. J. Fluid Mech., Vol. 114, 501-528.

Wigeland, R. A. 1978. Grid Generated Turbulence With and Without Rotation About the Streamwise Direction. Ph.D. Thesis, Illinois Institute of Technology.

END

DATE

FILMED

APR 13 1983